

Received: 10 June 2015 – Accepted: 14 June 2015 – Published: 03 July 2015

Correspondence to: K. Ashworth (ksashwor@umich.edu)

Published by Copernicus Publications on behalf of the European Geosciences Union.

GMDD

8, 5183–5234, 2015

FORest canopy atmosphere transfer (FORCAst) 1.0

K. Ashworth et al.

Title Page

Abstract

Introduction

Conclusions

References

Tables

Figures



Back

Close

Full Screen / Esc

Printer-friendly Version

Interactive Discussion



Abstract

Biosphere-atmosphere interactions play a critical role in governing atmospheric composition, mediating the concentration of key species such as ozone and aerosol, thereby influencing air quality and climate. The exchange of reactive trace gases and their oxidation products (both gas and particle phase) is of particular importance in this process. The FORCAsT (FORest Canopy AtmoSphere Transfer) one-dimensional model is developed to study the emission, deposition, chemistry and transport of volatile organic compounds (VOCs) and their oxidation products in the atmosphere within and above the forest canopy. We include an equilibrium partitioning scheme, making FORCAsT one of the few canopy models currently capable of simulating the formation of secondary organic aerosols (SOA) from VOC oxidation in a forest environment. We evaluate the capability of FORCAsT to reproduce observed concentrations of key gas-phase species and report modeled SOA concentrations within and above a mixed forest at the University of Michigan Biological Station (UMBS) during the Community Atmosphere-Biosphere Interactions Experiment (CABINEX) field campaign in summer 2009. We examine the impact of two different gas-phase chemical mechanisms on modelled concentrations of short-lived primary emissions, such as isoprene and monoterpenes, and their oxidation products. While the two chemistry schemes perform similarly under high-NO_x conditions, they diverge at the low levels of NO_x at UMBS. We identify peroxy radical and alkyl nitrate chemistry as the key causes of the differences, highlighting the importance of this chemistry in understanding the fate of biogenic VOCs (bVOCs) for both the modelling and measurement communities.

1 Introduction

Exchanges of energy and mass between the biosphere and atmosphere play a crucial role in the Earth system. These interactions control the physical and chemical properties of the atmosphere, which in turn influence the characteristics of the land surface

GMDD

8, 5183–5234, 2015

FORest canopy atmosphere transfer (FORCAsT) 1.0

K. Ashworth et al.

Title Page

Abstract

Introduction

Conclusions

References

Tables

Figures



Back

Close

Full Screen / Esc

Printer-friendly Version

Interactive Discussion



point models that explicitly consider the canopy space and its processes (e.g. CACHE, Forkel et al., 2006; Bryan et al., 2012; SOSA, Boy et al., 2011; CAFE, Wolfe and Thornton, 2011; MLC-Chem, Ganzeveld et al., 2002). These models range in complexity in terms of both vertical resolution and the chemical and physical mechanisms that are included.

Here, we describe the canopy model FORCA_{ST} (FORest Canopy-Atmosphere Transfer) which has been developed from the original Canopy Atmospheric CHEMistry Emission (CACHE) model (Forkel et al., 2006; Bryan et al., 2012). Major updates from CACHE include: (1) adding the CACM (Caltech Atmospheric Chemistry Mechanism) gas-phase chemistry scheme (Griffin et al., 2002, 2005; Chen and Griffin, 2005); (2) restructuring the code to facilitate switching between chemistry mechanisms using codes generated by the Kinetic PreProcessor (KPPv2.1; Sandu and Sander, 2006); and (3) incorporation of the MPMPO (Model to Predict the Multiphase Partitioning of Organics) aerosol module (Griffin et al., 2003, 2005; Chen and Griffin, 2005). We evaluate FORCA_{ST}'s performance against its predecessor, the CACHE model, and observations from the CABINEX intensive field campaign, conducted at the University of Michigan Biological Station (UMBS) during the summer of 2009.

2 Model description

The canopy exchange model FORCA_{ST} is a single column (1-D) model incorporating both atmospheric chemistry and dynamics and land surface modelling, based on the CACHE canopy exchange model (Forkel et al., 2006). Energy balances and radiative transfer within the canopy are calculated following the algorithms of the CUPID soil-plant-atmosphere model (Norman, 1979; Norman and Campbell, 1983).

From the atmospheric perspective, FORCA_{ST} includes parameterisations of all of the processes occurring within and above the canopy space: emissions, advection, deposition, turbulent (vertical) exchange, and chemical production and loss (Fig. 1b). One of the novel aspects of FORCA_{ST} is that it includes both the gas-phase chemistry

FORest canopy atmosphere transfer (FORCA_{ST}) 1.0

K. Ashworth et al.

Title Page

Abstract

Introduction

Conclusions

References

Tables

Figures



Back

Close

Full Screen / Esc

Printer-friendly Version

Interactive Discussion



FORest canopy atmosphere transfer (FORCAsT) 1.0

K. Ashworth et al.

Title Page

Abstract

Introduction

Conclusions

References

Tables

Figures

◀

▶

◀

▶

Back

Close

Full Screen / Esc

Printer-friendly Version

Interactive Discussion



levels representing the planetary boundary layer above. The thickness of the layers increases with height, permitting greater resolution in the canopy levels, which are further sub-divided into a trunk space and crown space. The height of the trunk space and the top of the crown space are set by the user for the specific location of interest.

The lower boundary of the column represents the land (soil) surface. In addition to the above-ground layers, the model includes 15 soil layers for computing soil heat and moisture storage and transfer to the atmosphere, as well as root extraction (Forkel et al., 2006).

As the CACHE model has been described extensively elsewhere (Forkel et al., 2006; Bryan et al., 2012), we mostly confine our descriptions to the improvements and updates to the original model although we give a brief summary of the main processes. We outline the general or default settings of FORCAsT simulations within the main text. Many of the parameters and boundary or initial conditions (e.g. canopy architecture, foliage properties, meteorological conditions, concentrations) in the model can be adjusted by the user for a specific site or time-period. The values for the simulation period used to evaluate FORCAsT are given in the accompanying Supplement, along with further information on the initialization and use of FORCAsT.

2.1 Canopy structure and radiative transfer

Following the parameterisations of the CUPID model (Norman, 1979; Norman and Campbell, 1983) FORCAsT simulates the transfer of radiation through the vegetation canopy, allowing an energy budget to be computed for each model level within the canopy space. Thus, prognostic leaf temperatures, and latent and sensible heat fluxes are determined for both sunlit and shaded foliage at each canopy level.

Incoming radiation at the top of the canopy is prescribed, either via user-provided radiation observations or by a default scheme within the code that includes provision for cloud coverage (based on an average fractional coverage specified by the user). Solar radiation is split between visible (0.4–0.7 μm) and near-infrared (0.7–4 μm), and the thermal radiation contribution (4–100 μm) is calculated on-line (Norman, 1979).

FORest canopy atmosphere transfer (FORCAst) 1.0

K. Ashworth et al.

Title Page

Abstract

Introduction

Conclusions

References

Tables

Figures



Back

Close

Full Screen / Esc

Printer-friendly Version

Interactive Discussion



The visible component of the incoming solar radiation is assumed equivalent to photo-synthetically active radiation (PAR) and is used to drive the biological vegetation processes linked to photosynthesis and biogenic emissions. Within the canopy, reflection, transmission and absorption of all incoming radiation wavelength bands and the total back-scattered or up-welling radiation is dependent on the canopy structure and the angle of the leaves relative to the incident radiation. The incoming solar radiation is further divided into direct and diffuse radiation based on the proportion of back-scattered radiation.

The canopy architecture is constructed during the initialisation routines within FOR-CAst. A leaf angle distribution (i.e. the area fraction of leaves within each canopy layer whose normal lines fall within a specified range of angles from the solar zenith angle) is calculated based on the total projected LAI of the canopy, and the fraction of the total LAI in each canopy layer (which may be set by the user via an input file). By default, the calculation assumes a spherical canopy (i.e. perfectly symmetrical in all directions) in terms of its response to incoming radiation, but this may also be altered via the input file. FORCAst currently considers 9 angle classes of sunlit leaves, and designates an additional (tenth) class to the shaded leaves within each layer. An initial attenuation factor for radiation within the canopy is then calculated based on this leaf angle distribution and a user-provided foliage clumping factor, describing the distribution of leaves along the branches, and hence the ease with which radiation can penetrate the canopy.

The effective area of leaf surface intercepting solar radiation is then calculated at each model timestep assuming a β -distribution relative to the solar zenith angle (Goel and Strebel, 1984) and a default azimuthal angle distribution (Strebel et al., 1985). Either of these distributions can be altered by the user to fit site-specific observations of canopy structure. This effective interception area for each angle class in each canopy layer provides the basis for the simulation of light attenuation within the canopy (based on Beer's Law), and of the absorption of thermal radiation at each model timestep. Leaves in the nine sunlit angle classes are assumed to receive components of both direct and diffuse radiation; shaded leaves receive only diffuse.

Radiation penetrating each canopy layer decays due to shading from leaves in the layers above. An energy balance is calculated for each leaf angle class within each canopy layer to determine leaf temperature and heat fluxes. Biogenic emissions, driven by PAR and leaf temperature, thus vary between layers and between angle classes within a single layer.

2.2 Emissions

Biogenic emissions of VOCs (bVOCs) from canopy vegetation are calculated on-line using the parameterised light and temperature dependencies developed by Guenther et al. (1995) and modified by Steinbrecher et al. (1999) to account for emissions from storage pools. Pool emissions are dependent on temperature alone and are characteristic of most terpenoids, although isoprene is only emitted via direct synthesis. Site-specific direct synthesis and pool emission factors are prescribed for different vegetation types and bVOCs.

Emissions flux (F ; $\text{nmol m}^{-2} \text{s}^{-1}$) are calculated for each leaf-angle class and summed over each layer in the canopy crown space using prognostic leaf temperature and accounting for sunlit and shaded leaves in each level at every model timestep.

$$\text{Synthesis (direct) emissions: } F = \text{LAI} \cdot \varepsilon \cdot \gamma_{\text{TS}} \cdot \gamma_{\text{LS}} \quad (4)$$

where LAI is the leaf area index in each leaf-angle class and layer, ε is the emission factor or base emission rate (i.e. the emission rate at standard conditions of 30°C and incoming PAR of $1000 \mu\text{mol m}^{-2} \text{s}^{-1}$) and γ_{TS} and γ_{LS} are scaling factors accounting for the actual leaf temperature and incoming radiation respectively. The scaling factors are calculated as:

$$\text{Temperature scaling factor: } \gamma_{\text{TS}} = \frac{\exp\left(\frac{C_{\text{T1}}(T_{\text{L}} - T_{\text{S}})}{R \cdot T_{\text{L}} \cdot T_{\text{S}}}\right)}{x + \exp\left(\frac{C_{\text{T2}}(T_{\text{L}} - T_{\text{M}})}{R \cdot T_{\text{L}} \cdot T_{\text{S}}}\right)} \quad (5)$$

5191

FORest canopy atmosphere transfer (FORCAst) 1.0

K. Ashworth et al.

[Title Page](#)[Abstract](#)[Introduction](#)[Conclusions](#)[References](#)[Tables](#)[Figures](#)[◀](#)[▶](#)[◀](#)[▶](#)[Back](#)[Close](#)[Full Screen / Esc](#)[Printer-friendly Version](#)[Interactive Discussion](#)

where C_{T1} , C_{T2} and x are empirically determined coefficients (95 000, 230 000 J mol⁻¹ and 0.926 respectively). T_L is the leaf temperature, T_S is a standard temperature (here taken as 303 K), and T_M is an optimum temperature (here set to 314 K). R is the ideal gas constant (8.314 JK⁻¹ mol⁻¹).

$$5 \text{ Light scaling factor: } \gamma_{LS} = \frac{\alpha \cdot C_L \cdot \text{PAR}}{\sqrt{1 + \alpha \cdot \text{PAR}^2}} \quad (6)$$

where C_L and α are empirically determined coefficients (1.1066 and 0.0027 respectively). PAR ($\mu\text{mol m}^{-2} \text{s}^{-1}$) is that reaching the leaf surface.

$$\text{Pool emissions: } F = \text{LAI} \cdot \varepsilon \cdot \gamma_{TP} \quad (7)$$

10 where γ_{TP} is the temperature correction factor accounting for the actual conditions, calculated as:

$$\text{Temperature correction factor: } \gamma_{TP} = \exp(\beta(T_L - T_S)) \quad (8)$$

where constant β is determined from observations (typically 0.09 K⁻¹) and T_S is taken as 293 K.

2.3 Advection

15 Traditionally, box and 1-D canopy models do not include advection as they are not designed or intended to be atmospheric transport models. However, without additional advective sources or sinks of heat or mass, many such models cannot reliably capture observed fluctuations in concentrations of primary emitted species and their immediate oxidation products, which may accumulate in the column.

layer on the leaf surface (level dependent), and the mesophyll and cuticular resistances (species dependent), and stomatal resistance (level and species dependent). The soil or surface resistance is modelled after Gao et al. (1993).

Deposition is assumed to occur at a rate dependent on species-specific Henry's Law coefficient, diffusivity relative to water vapour and a nominal "reactivity" relative to ozone. The ozone-relative reactivity has been increased for oxygenated VOCs and bVOC oxidation products following Karl et al. (2010) to account for enhanced uptake due to reactions occurring within plant cells.

As FORCAsT includes a full multi-level representation of vegetation structure, the processes governing deposition rates are explicitly incorporated. In particular, stomatal conductance for each leaf angle class in each canopy layer is calculated according to the canopy environment at each time step, accounting for changes in temperature, light levels above and within the canopy, and vapour pressure deficit. Soil resistances are likewise calculated at each timestep based on the temperature and soil moisture profile at that time.

Deposition velocities of gases and particles are calculated by FORCAsT before being passed to the chemistry scheme, where they are included as a loss term in the computation of reaction rates. The mass of a species lost through deposition is calculated from its deposition velocity or potential and its atmospheric concentration within any particular vertical layer.

As the simulation of stomatal conductance within FORCAsT occurs on-line, this provides the potential to estimate the flux of any species into the vegetation, allowing simulation of damage to plant cells due to the uptake of powerful oxidising agents such as ozone. This capability will be utilised in future studies.

2.5 Turbulent exchange

In FORCAsT, vertical turbulent exchange of mass and energy follows traditional *K* theory (Blackadar, 1962). Mixing within and above the canopy is simulated using the parameterisations of Baldocchi (1988) and Gao et al. (1993), respectively. The resulting

FORest canopy atmosphere transfer (FORCAsT) 1.0

K. Ashworth et al.

Title Page

Abstract

Introduction

Conclusions

References

Tables

Figures



Back

Close

Full Screen / Esc

Printer-friendly Version

Interactive Discussion



**FORest canopy
atmosphere transfer
(FORCAsT) 1.0**

K. Ashworth et al.

[Title Page](#)[Abstract](#)[Introduction](#)[Conclusions](#)[References](#)[Tables](#)[Figures](#)[Back](#)[Close](#)[Full Screen / Esc](#)[Printer-friendly Version](#)[Interactive Discussion](#)

vertical profiles are further modified to improve the simulated exchange of heat and trace gases by constraining the friction velocity with sonic anemometer observations near the canopy following Bryan et al. (2012). For the simulation period presented here (see Sect. 3 for details), sonic data are incorporated at two heights (20.6 m – roughly the top of the canopy, and 36.94 m – the top of the PROPHET flux measurement tower at UMBS; see Sect. 3). The vertical exchange coefficient (K in Eqs. 2.1–2.3) within the crown space is calculated by linear interpolation between the modelled value at the crown base and the value estimated from sonic data at the top of the canopy, following the approach of Stroud et al. (2005). The same procedure is then performed between the top of the canopy and top of the tower, and the top of the tower value is linearly interpolated to the value at 1 km modelled using Gao et al. (1993). Bryan et al. (2012) demonstrate that the limitations of traditional K theory within and just above the canopy make this method necessary to capture the observed vertical exchange and distribution of heat and mass.

2.6 Gas-phase chemistry

In FORCAsT, gas-phase chemistry can be calculated using either the Regional Atmospheric Chemistry Mechanism (RACM; Stockwell et al., 1997; Geiger et al., 2003) or CACM mechanisms, but aerosol partitioning is only available when CACM is used, via the MPMPO equilibrium-partitioning model (Griffin et al., 2003, 2005; Chen et al., 2006). The subroutines and modules within the CACM model included here have been generated using the Kinetic PreProcessor (KPP; Sandu and Sander, 2006), facilitating the use of other chemistry schemes within FORCAsT.

2.6.1 RACM

The version of RACM included in FORCAsT incorporates the key reactions of the Mainz Isoprene Mechanism (Pöschl et al., 2000) as described by Geiger et al. (2003). The concentrations of 84 gas-phase species are calculated at 1 min timesteps. The scheme

includes 249 reactions. Changes to RACM since its original description by Stockwell et al. (1997) are listed in Tables B1–B2 in the Supplement.

2.6.2 CACM

In order to achieve an improved representation of condensable species and simulate SOA formation within the canopy, we add the CACM (Griffin et al., 2002, 2005; Chen and Griffin, 2005; Chen et al., 2006) gas-phase chemical mechanism because of its explicit treatment of SOA-relevant chemical species. CACM uses a mechanistic approach to simulate VOC-NO_x-HO_x chemistry while tracking condensable species that contribute to SOA. This represents an intermediate complexity approach between those of a highly lumped, simplified mechanism such as RACM and a fully explicit chemical mechanism such as the University of Leeds Master Chemical Mechanism (MCM) (Jenkin et al., 2003; Saunders et al., 2003). In principle, the MCM approach is most rigorous, but such a mechanism is computationally expensive, and many of the required reaction rates, products, and thermodynamic parameters are still not accurately known. CACM is a condensed version of MCM that simulates ozone chemistry as well as formation of individual organic oxidation products that are capable of forming SOA. The version of CACM incorporated into FORCAST includes the original mechanism of Griffin et al. (2002) with updates of Griffin et al. (2005) and addition of explicit treatments for SOA formation from the monoterpenes α -pinene, β -pinene, and *d*-limonene of Chen and Griffin (2005). It includes 300 prognostic species and 620 chemical reactions, with a full description listed in Tables A1–A2 of the Supplement. To simulate SOA, gas-phase species in CACM are categorized into condensable and non-condensable groups according to experimental or estimated vapour pressures or solubility.

2.6.3 Update of the CACM mechanism for low-NO_x conditions

The performance of the original CACM mechanism (i.e. as described by Griffin et al., 2002, 2005; Chen et al., 2005, and referred to as CACM0.0 hereafter) was tested for

GMDD

8, 5183–5234, 2015

FORest canopy atmosphere transfer (FORCAST) 1.0

K. Ashworth et al.

Title Page

Abstract

Introduction

Conclusions

References

Tables

Figures



Back

Close

Full Screen / Esc

Printer-friendly Version

Interactive Discussion



**FORest canopy
atmosphere transfer
(FORCAsT) 1.0**

K. Ashworth et al.

Title Page

Abstract

Introduction

Conclusions

References

Tables

Figures



Back

Close

Full Screen / Esc

Printer-friendly Version

Interactive Discussion



would be similarly well modelled. However, as is evident from Fig. 2c, which shows the mixing ratio of methyl vinyl ketone plus methacrolein (lumped as a single species in the RACM mechanism although treated separately by CACM0.0, and referred to hereafter as MVK-MCR), neither chemistry mechanism reproduces either the diurnal profile or the absolute concentrations of MVK-MCR in the canopy space. In both cases, the modelled concentrations are far higher than those observed and there is a tendency for accumulation within the canopy over the course of the two days. MVK-MCR concentrations on the second day of the RACM simulation are substantially lower than those modelled by CACM0.0, but are still a factor of 2–3 higher than observations.

CACM0.0 displays the same difficulties with formaldehyde (Fig. 2d), over-estimating the concentration at the top of canopy by a factor of 4–5. RACM performs much better in terms of capturing the absolute concentrations but fails to reproduce the diurnal profile seen in the measurements on the second day of the simulation period.

Many of the differences in modelled concentrations between the two chemistry schemes were found to be attributable to the availability of oxidants in the two simulations. Following an initial sharp decline in NO_2 (Fig. 2e), which is also evident in the observations and the RACM simulation, NO_x concentrations in CACM0.0 fail to recover indicating that loss rates far exceed the rates of production or recycling of NO_x in the scheme. NO mixing ratios (Fig. 2f) behave similarly, following the measured concentrations and those simulated by RACM early on the first day, but failing to recover once exhausted.

The picture is more complex when considering the HO_x oxidants. CACM0.0 and RACM produce very similar mixing ratios of the OH radical (Fig. 2h), although both appear to fall well below measured concentrations. The final panels of Fig. 2 show concentrations of HO_2 (Fig. 2i) and HO_2^* (the sum of HO_2 and the OH^+ isoprene-derived peroxy radicals; Fig. 2j). In both cases, the model concentrations are displayed against measurements of HO_2 made at the site. It is thought that HO_2 sampling instruments detect both HO_2 and these peroxy radicals on the same channel, and that modelled output of HO_2^* is therefore more appropriate to use for comparison (Griffith et al., 2013;

Fuchs et al., 2011). HO₂ concentrations for both chemistry models are well below those measured (as would be expected if the observations include the peroxy radicals), but again CACM0.0 mixing ratios are lower than those in RACM, from the point on 04 August when NO_x levels reach zero in the CACM0.0 simulation. Interestingly, however, while RACM mixing ratios of HO₂* agree well with the measurement data, the combined concentrations in the CACM0.0 scheme exceed the measured values by a factor of 20–30, suggesting a significant over-estimation of isoprene-derived peroxy radicals.

The time of divergence of modelled concentrations coincides with meteorological changes at the site. As outlined in Sects. 3 and 4, the prevailing conditions at UMBS changed with the passage of a cold front on the morning of the 04 August, bringing cooler cleaner air from the north. Around mid-morning of the 04 August therefore marks a transition from what could be considered a high-NO_x to a low-NO_x regime at the site, suggesting that CACM0.0 fails to represent low-NO_x VOC oxidation chemistry effectively. Previous studies using and evaluating the CACM scheme (see for example Griffin et al., 2002; Chen et al., 2007, 2010) were all conducted in regions and time periods when NO_x levels were high relative to bVOC concentrations. Under such conditions, CACM0.0 has been shown to perform well. In addition, the mechanism was developed and tested in a region in which the VOC budget is dominated by anthropogenic sources, with the bVOC contribution predominantly from monoterpenes rather than isoprene. Applying the model for this two-day period at UMBS, which can be characterised as a combination of low NO_x and high isoprene concentrations therefore represented a profound change from previous simulations.

Figure 2 suggests that the key difference between the mechanisms is the production and loss of peroxy radicals formed from the initial oxidation reactions of VOCs. The main chemical sinks for peroxy radicals are through reactions with NO, HO₂ and with other peroxy radicals (see e.g. Atkinson and Arey, 2003; Jenkin et al., 1997; Perring

**FORest canopy
atmosphere transfer
(FORCAsT) 1.0**

K. Ashworth et al.

Title Page

Abstract

Introduction

Conclusions

References

Tables

Figures

◀

▶

◀

▶

Back

Close

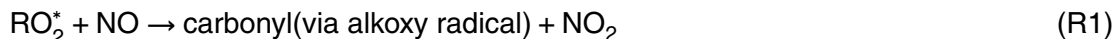
Full Screen / Esc

Printer-friendly Version

Interactive Discussion



et al., 2013):



Sensitivity studies were conducted for high- NO_x conditions, in which the performance of CACM0.0 was found to be closely comparable to that of the RACM scheme, indicating that the discrepancies shown in Fig. 2 were due to the low levels of NO_x at UMBS (results not shown). These studies strongly suggested that the source of the discrepancy was the relative rates of Reactions (R1)–(R4). This hypothesis is consistent with current understanding of the difference in radical termination reactions at high and low- NO_x levels. When NO_x concentrations are high relative to those of VOCs, the RO_2^* peroxy radicals formed from the initial oxidation of VOCs are oxidised to stable species through their reactions with NO (Reactions R1 and R2). At relatively lower levels of NO_x , termination reactions of the peroxy radicals with HO_2 (Reaction R3) and other RO_2^* (Reaction R4) dominate. Evidence from recent field campaigns and laboratory experiments indicates that the self- and cross-reactions between RO_2^* radical species (Reaction R4) are of particular importance in locations where the $\text{VOC} : \text{NO}_x$ ratio is very high (such as forested ecosystem in remote environments; see e.g. Whalley et al., 2014; Wolfe et al., 2014; Perring et al., 2013; Peeters et al., 2009).

The original isoprene chemistry in CACM0.0 (Griffin et al., 2002) was based on knowledge that is now almost two decades old and, unlike the monoterpene chemistry (Chen and Griffin, 2005), has not been updated. We update CACM0.0 to include some recent advances in modelling low- NO_x atmospheric VOC oxidation.

CACM0.0 relies on the NO reactions to continue the degradation of VOCs after the initial oxidation by OH, O_3 or NO_3 , with few peroxy radicals channelled through the HO_2/RO_2 pathways, even at very low concentrations of NO. Once NO_x levels fall, the

**FORest canopy
atmosphere transfer
(FORCAst) 1.0**

K. Ashworth et al.

Title Page

Abstract

Introduction

Conclusions

References

Tables

Figures



Back

Close

Full Screen / Esc

Printer-friendly Version

Interactive Discussion



rates of these reactions slow and peroxy radicals accumulate in the system, resulting in further depletion of NO and feeding back to further accumulation of peroxy radicals.

The rates of equivalent or similar reactions involving peroxy radicals in the CACM0.0 mechanism were compared against those in RACM and MCM v3.2 (<http://mcm.leeds.ac.uk/MCM/>). The rates of $\text{RO}_2^* + \text{NO}$ reactions were similar across all mechanisms, as might be expected given that such reactions are well-studied and well-constrained, and that CACM0.0 performed similarly to RACM under high- NO_x conditions. The HO_2 reaction rates were generally lower (by a factor of around 3) in the CACM0.0 scheme, accounting in part for slightly higher HO_2 concentrations in the CACM0.0 simulation under high- NO_x conditions (not shown).

The most substantial discrepancies between the mechanisms were the rates of the $\text{RO}_2^* + \text{RO}_2^*$ reactions. Direct comparison with the RACM scheme was difficult as CACM0.0 employs the technique of using a generic peroxy radical species (referred to as RO_2T – see Table A2) that is effectively the sum of all peroxy radicals to represent all possible permutations of Reaction (R4). There are fewer distinct peroxy radical species in RACM, and other than the methyl and isoprene-derived peroxy radicals, there are no self- or cross-reactions included. Comparison with the MCM showed that other than for the reactions involving radicals produced from monoterpene oxidation (which were updated more recently by Chen et al., 2005) the reaction rates used in CACM0.0 were several orders of magnitude too low. The reaction rates of the peroxy radical reactions with HO_2 (Reaction R3) and RO_2^* (Reaction R4) were therefore increased to better match those in the MCM (see Table A2 of the Supplement).

Recent data from field campaigns also suggests that the formation and loss of organic nitrates produced from alkyl peroxy radicals play an important role in governing nitrogen cycling and availability over relatively short timescales particularly in low- NO_x environments (Beaver et al., 2012; Brown et al., 2010; Browne et al., 2010; Perring et al., 2013). While the CACM0.0 mechanism included formation of alkyl nitrates from the reactions of many of the alkyl peroxy radicals with NO, not all of the isoprene peroxy radicals produced nitrates. Given the relative abundance of isoprene at this site,

FORest canopy atmosphere transfer (FORCAst) 1.0

K. Ashworth et al.

Title Page

Abstract

Introduction

Conclusions

References

Tables

Figures



Back

Close

Full Screen / Esc

Printer-friendly Version

Interactive Discussion



the clear over-production (or reduced loss) of isoprene peroxy radicals, and the low NO_x conditions, the products of these reactions were altered to include the formation of isoprene nitrates (see Table A2 of the Supplement).

The subsequent reactions of alkyl nitrates with OH, which release NO_2 at timescales likely to be relevant to in-canopy chemistry, included in the original scheme (Griffin et al., 2002) but later removed (Griffin et al., 2005), were re-introduced. Equivalent reactions for the new isoprene nitrates were also added, as nitrates formed from bVOCs are known to have particularly short lifetimes with respect to the OH radical (Müller et al., 2014; Perring et al., 2013; Paulot et al., 2009), suggesting that these reactions occur on timescales likely to be of relevance to in-canopy chemistry.

New laboratory experiments have also demonstrated that photolysis of isoprene-derived nitrates may occur at a timescale competitive with their reactions with the OH radical (Müller et al., 2014). The breakdown of the isoprene nitrates via photolysis has therefore also been included, with photolysis rates following the suggestions of Müller et al. (2014) (see Table A2 of the Supplement).

As shown in Fig. 2d, CACM0.0 also produces too much formaldehyde compared to both the observations and the RACM scheme. While the initial problem may stem from excessive reaction rates or formaldehyde yields from $\text{RO}_2^* + \text{NO}$ reactions, it was found that bias increases were larger under low- NO_x than high- NO_x conditions, suggesting this is associated with $\text{RO}_2^* + \text{RO}_2^*$ and $\text{RO}_2^* + \text{HO}_2$ reactions. When NO_x is abundant relative to VOCs, the reaction with NO dominates with minor contributions from HO_2 and RO_2^* pathways (Reactions R1 and R2). In low- NO_x environments, the competing HO_2 and RO_2^* reactions form the main sink of peroxy radicals (Reactions R3 and R4). As reactions between peroxy radicals and HO_2 do not form carbonyl compounds as first-generation products, overall yields of aldehydes and ketones are reduced when NO_x levels are low and a greater proportion of oxidation occurs via reaction with HO_2 (see, e.g., Sumner et al., 2001). Experiments of isoprene peroxy radical reactions conducted under high- NO_x and NO_x -free conditions, for example, suggest that the overall

**FORest canopy
atmosphere transfer
(FORCAst) 1.0**

K. Ashworth et al.

Title Page

Abstract

Introduction

Conclusions

References

Tables

Figures



Back

Close

Full Screen / Esc

Printer-friendly Version

Interactive Discussion



yield of formaldehyde is around 0.57 when NO_x is abundant; dropping to around 0.34 when no NO_x is present (Miyoshi et al., 1994).

Although the peroxy radical $+\text{HO}_2$ reactions initially form organic peroxides, subsequent photolysis releases carbonyls and HO_x . The reaction scheme in CACM0.0 combines these into a single step with peroxy radicals reacting with HO_2 to form aldehydes (mostly formaldehyde) immediately, in addition to a proxy species that then photolyses to recycle HO_x . By contrast, RACM forms an organic peroxide that can then photolyse to form an aldehyde and HO_x , with formaldehyde only being produced from the peroxide produced from methane oxidation. While the approach in CACM0.0 should in theory permit better aldehyde speciation without the introduction of numerous separate photolysis reactions, the overall effect is to increase the production of formaldehyde and to alter the time at which it is produced. As photolysis only occurs during daylight hours, the inclusion of this as a separate reaction could be expected to introduce a diurnal profile that is currently absent from CACM0.0 formaldehyde concentrations.

The peroxy radical reactions in CACM0.0 were modified as outlined above to bring them closer in line with those included in RACM. The formaldehyde yield from the peroxy radical $+\text{HO}_2$ reactions was set to zero, and a yield of unity added to the photolysis reactions of the proxy species formed from the peroxy radical $+\text{HO}_2$ reactions. The photolysis rate of this reaction was also increased to match that in the RACM mechanism.

These updates to CACM0.0, hereafter referred to as CACM, are included in FORCAST 1.0.

2.7 Aerosol partitioning

One of the most significant capabilities of FORCAST 1.0 is the inclusion of the partitioning of condensable species to the particle phase. Of the 300 prognostic species in CACM, 99 are treated as condensable in MPMPO (highlighted in Table A3 of the Supplement). For biogenic SOA precursors, CACM includes explicit gas-phase chemistry for α -pinene, β -pinene, and d -limonene (Chen and Griffin, 2005); other monoterpenes

GMDD

8, 5183–5234, 2015

FORest canopy atmosphere transfer (FORCAST) 1.0

K. Ashworth et al.

Title Page

Abstract

Introduction

Conclusions

References

Tables

Figures



Back

Close

Full Screen / Esc

Printer-friendly Version

Interactive Discussion



FORest canopy atmosphere transfer (FORCAst) 1.0

K. Ashworth et al.

Title Page

Abstract

Introduction

Conclusions

References

Tables

Figures



Back

Close

Full Screen / Esc

Printer-friendly Version

Interactive Discussion



are lumped into a low SOA yield or a high SOA yield group, represented by α -terpineol and δ -terpinene, respectively (Griffin et al., 2002). Explicit formation of SOA from isoprene is not considered in this version of MPMPO, driven by the CACM gas-phase mechanism (hereafter referred to as CACM-MPMPO). However, oxidation reactions of methyl vinyl ketone and methacrolein, two major oxidation products of isoprene, form keto-propanoic acid and oxalic acid, respectively, which are considered condensable and form SOA in CACM-MPMPO. Anthropogenic SOA and primary organic aerosols (POA) are also included in MPMPO (Griffin et al., 2003, 2005). For the simulations of UMBS during the CABINEX campaign presented here, POA concentration is assumed to be a constant value of $0.5 \mu\text{g m}^{-3}$ and anthropogenic VOC concentrations are set to zero.

Condensable species formed from VOC oxidation in CACM create a “reservoir” of potential SOA. In MPMPO, the 99 condensable species are lumped into 12 surrogate species according to their structures, sources (biogenic or anthropogenic), volatilities, and dissociative capabilities. These surrogate species are the original S1 to S9 groups described in Griffin et al. (2003), an updated S10 group described in Griffin et al. (2005), a new S11 group for β -pinene oxidation product 2,10-dinitrato-pinane (Chen et al., 2006), and a new S12 non-volatile group representing dimers formed from multifunctional acid species generated from oxidation of monoterpenes (Chen et al., 2006). Characteristics, surrogate species, and list of species for each surrogate group are summarized in Table A3 of the Supplement.

The MPMPO aerosol module calculates the partitioning of the CACM gas-phase condensable oxidation products. Absorption into the organic phase is governed by the an absorption coefficient, $K_{\text{om},i}$ ($\text{m}^3 \mu\text{g}^{-1}$) (Pankow, 1994):

$$K_{\text{om},i} = \frac{O_i}{G_i M_o} = \frac{RT}{\text{MW}_{\text{om}} 10^6 \gamma_i \rho_{L,i}^o} \quad (11)$$

where O_i ($\mu\text{g m}^{-3}$ air) and G_i ($\mu\text{g m}^{-3}$ air) are the organic aerosol- and gas-phase concentrations of surrogate species i , respectively, M_o ($\mu\text{g m}^{-3}$ air) is the

total organic aerosol-phase concentration, R is the ideal gas constant ($8.206 \times 10^{-5} \text{ m}^3 \text{ atm mol}^{-1} \text{ K}^{-1}$), T is temperature (K), MW_{om} is the average molecular weight of the organic phase (g mol^{-1}), γ_i is the activity coefficient of surrogate i , and $p_{L,i}^{\circ}$ is the pure component vapor pressure (atm) of surrogate i at temperature T . The method of Myrdal and Yalkowsky (1997) calculates $p_{L,i}^{\circ}$, and the UNIFAC method is employed to calculate activity coefficients γ_i (Fredenslund et al., 1977; Smith and Van Ness, 1987; Saxena and Hildemann, 1996; Pankow et al., 2001; Seinfeld et al., 2001).

The partitioning between the gas and the aqueous phase is determined by

$$A_i = \frac{G_i(\text{LWC})H_i}{\gamma_{\text{aq},i}} \quad (12)$$

where A_i ($\mu\text{g m}^{-3}$) is the aqueous-phase concentration of surrogate species i , LWC ($\mu\text{g H}_2\text{O m}^{-3}$ air) is the liquid water content in the aqueous phase, H_i ($\mu\text{g } \mu\text{g}^{-1} \text{ H}_2\text{O}$) is the Henry's Law coefficient of surrogate species i , and $\gamma_{\text{aq},i}$ is the activity coefficient (normalized by that at infinite dilution) of surrogate species i in the aqueous phase. The group contribution method of Suzuki et al. (1992) is used to estimate the Henry's Law coefficients H_i . The UNIFAC method is employed to calculate activity coefficients $\gamma_{\text{aq},i}$. The liquid water content due to the presence of aqueous phase organics is determined using the Zdanovskii–Stokes–Robinson (ZSR) method (Meng et al., 1998; Pun et al., 2002). Total aerosol liquid water content (ALWC) associated with inorganic and organic phases is an input to the MPMPO module and is needed to determine organic aerosol aqueous-phase concentrations. For the simulations presented here, we used hourly ALWC calculated using the hygroscopicity parameter, κ which is based on observed CCN concentrations at 0.3% supersaturation and observed particle size distributions during CABINEX (VanReken et al., 2015).

For the aqueous phase, equilibrium is also constrained by dissociation of the dissolved organic species. The concentrations of the singly charged ion from surrogate species i , A_{1i} ($\mu\text{g m}^{-3}$ air), and the concentration of the doubly charged ion from surro-

Title Page

Abstract

Introduction

Conclusions

References

Tables

Figures



Back

Close

Full Screen / Esc

Printer-friendly Version

Interactive Discussion



gate species i , A_{2i} ($\mu\text{g m}^{-3}$ air), can be represented as

$$A_{1i} = \frac{K_{1i}A_i(MW_i - MW_{\text{H}^+})}{[\text{H}^+]MW_i} \quad (13)$$

$$A_{2i} = \frac{K_{2i}A_i(MW_i - 2MW_{\text{H}^+})}{[\text{H}^+]MW_i} \quad (14)$$

where $[\text{H}^+]$ ($\text{mol kg}^{-1} \text{H}_2\text{O}$) is the proton concentration in the aqueous phase, and K_{1i} and K_{2i} ($\text{mol kg}^{-1} \text{H}_2\text{O}$) are the dissociation constants, which are estimated using structure-activity relationships (Harris and Hayes, 1982; Schwarzenbach et al., 1993).

3 Evaluation

The performance of FORCAST was evaluated with output from the CACHE canopy and chemistry model described in Bryan et al. (2012) and observations from UMBS during the CABINEX campaign in 2009 (*Atmos. Chem. Phys.*, special issue: Williams et al., 2011). This intensive field campaign was primarily focused at the PROPHET flux tower with further measurements made at the nearby Ameriflux tower. Full details of this field measurement site and the PROPHET tower can be found in Carroll et al. (2001), with the 2009 campaign described in Kanawade et al. (2011), Kim et al. (2011), Steiner et al. (2011), Zhang et al. (2012), Bryan et al. (2012), Griffith et al. (2013), and Van Reken et al. (2015).

The results presented here are based on a two-day model simulation for 04–05 August 2009, coinciding with the simulation period in Bryan et al. (2012). The driving meteorology, land surface and vegetation characteristics are derived from UMBS measurements and are identical to those used in the previous study. Initial and boundary conditions were also set following Bryan et al. (2012) with the addition of aerosol measurements (Van Reken et al., 2015) to allow full and robust comparison of the models'

Title Page

Abstract

Introduction

Conclusions

References

Tables

Figures



Back

Close

Full Screen / Esc

Printer-friendly Version

Interactive Discussion



than 21 °C on both days, slightly below the average high temperature of 22 °C for the CABINEX period (Bryan et al., 2012).

The change in wind direction also resulted in different chemical conditions at the site, with southerly air mass bringing anthropogenic pollutants from Detroit and Chicago. Air masses from the North are associated with clean (low-NO_x) conditions.

4 Results

4.1 Air temperature

The air temperature (Fig. 3) modeled by the energy balance routines in FORCAsT shows a typical diurnal cycle and is generally in reasonable agreement with the observed temperatures in the canopy. However, during the first 6 h of the simulation period, modeled temperatures are well below those experienced at UMBS. The passage of the frontal system from the north discussed above (Sect. 3) brought cooler temperatures to the site. Conditions prior to this had been relatively stagnant with temperatures remaining elevated overnight due to a warm air mass over the site. As FORCAsT is a 1-D model, without prescriptive meteorology, it cannot be expected to capture this. However, the canopy energy balance also appears to over-predict canopy air temperatures at all heights during the middle of the day and also fails to reproduce accurately the variation of temperature with height overnight within the canopy. Specifically, simulated overnight temperatures are 2–3 °C above those observed at 20.4 and 34 m.

The discrepancy between the modeled and observed air temperatures during the first 8 h of the simulation period is sufficiently great to affect simulated emission and reaction rates (see Sect. 4.2). The time until 08:00 EST (Eastern Standard Time) on 04 August is therefore treated as a spin-up period and not included in our evaluation of model performance.

GMDD

8, 5183–5234, 2015

FORest canopy atmosphere transfer (FORCAsT) 1.0

K. Ashworth et al.

Title Page

Abstract

Introduction

Conclusions

References

Tables

Figures



Back

Close

Full Screen / Esc

Printer-friendly Version

Interactive Discussion



4.2 Gas-phase chemistry

The gas-phase chemistry scheme was modified to improve performance under low- NO_x conditions. Section 4.2.1 compares output from FORCAsT (i.e. the updated CACM scheme) against UMBS observations and RACM output data. FORCAsT is also evaluated under high- NO_x conditions to ensure that the modifications to CACM0.0 do not adversely affect its performance in these situations. The same two-day period was modelled as a high- NO_x environment by artificially advecting NO_2 throughout the simulation period. The rate of NO_2 advection to the site was consistent with an assumption of continual southerly winds bringing pollution from Detroit, as outlined by Bryan et al. (2012). The results of these simulations are presented in Sect. 4.2.2.

4.2.1 Low- NO_x

Figure 4 shows concentrations of key species involved in VOC oxidation at the top of the tower (~ 35 m) for 04–05 August 2009 as observed and modeled with RACM and the updated CACM-MPMPO chemistry mechanisms. The grey shaded region in all Figures denotes the spin-up period as explained above in Sect. 3.

FORCAsT reproduces both the magnitude and the diurnal profile of the observed isoprene concentrations reasonably well (Fig. 4a). However, the modelled mixing ratio of isoprene is higher than that observed during the middle of the day and this may be due to an over-estimation of temperature (Fig. 3). While the daytime discrepancies between modelled and measured concentrations can be ascribed to incorrect emissions, the biggest difference occurs during the night. As isoprene emissions are light dependent, night-time emissions are zero and observed concentrations approach zero. In both chemical mechanisms, concentrations are still about 1 ppb at night, suggesting inadequate oxidation in both of the chemistry scheme(s), either at night (possibly due to insufficient NO_3 radical concentrations) or during the late afternoon (resulting in an accumulation of isoprene that persists overnight). Both mechanisms show virtually

FORest canopy atmosphere transfer (FORCAsT) 1.0

K. Ashworth et al.

Title Page

Abstract

Introduction

Conclusions

References

Tables

Figures



Back

Close

Full Screen / Esc

Printer-friendly Version

Interactive Discussion



identical diel cycles, demonstrating the relative insignificance of chemistry compared with other canopy processes over the time and spatial scales involved.

Monoterpene concentrations (Fig. 4b) are similarly relatively well reproduced by FORCAST, as might be expected given that they are also a primary emission in the canopy. Both chemistry mechanisms simulate the same diurnal profile, with maximum concentrations at night when chemistry is slow and vertical mixing out of the canopy is negligible.

Concentrations of MVK-MCR simulated by FORCAST (Fig. 4c) with all chemical mechanism options remain well above those observed (by a factor of ~ 3 – 5) and show a tendency to accumulate over the course of the day. The updates to the CACM scheme have brought the diurnal profile of MVK-MCR more into line with that with that of RACM, although neither scheme captures the observed pattern well. Although production is initially more rapid in CACM, mixing ratios are not significantly above those in CACM0.0.

The elevated concentrations of MVK-MCR are most likely the result of the over-production of peroxy radicals, with many of the peroxy radical reactions in CACM producing further peroxy radicals. While both methyl vinyl ketone and methacrolein are direct reaction products of the initial oxidation of isoprene by O_3 , their primary sources are the reactions of isoprene-derived peroxy radicals. Figure 5b and d shows the concentrations of the peroxy radicals produced in the initial oxidation of isoprene by the OH radical, and of the summed peroxy radicals (RO₂T) in CACM with those simulated by RACM for comparison. The mixing ratios of peroxy radicals in the CACM simulations are a factor of 2–3 above those estimated by the RACM mechanism (Fig. 5a). While the improvements made to CACM0.0 bring both the magnitude and diurnal profile of the peroxy radical concentrations in closer agreement with the RACM scheme, CACM still shows a tendency to over-produce and/or under represent their losses. The diurnal profiles of mixing ratios of the isoprene +OH-derived peroxy radicals are in close agreement and strongly reflect the diel cycle of isoprene emissions (Fig. 5c). CACM concentrations, although well below those simulated by CACM0.0, still exceed those generated in RACM by 100–200%. Although the model output cannot be directly eval-

FORest canopy atmosphere transfer (FORCAst) 1.0

K. Ashworth et al.

Title Page

Abstract

Introduction

Conclusions

References

Tables

Figures



Back

Close

Full Screen / Esc

Printer-friendly Version

Interactive Discussion



uated due to the lack of observations, the relative overestimation of MVK-MCR concentrations in CACM compared to both measured levels and those simulated by the RACM scheme, suggest that these radicals are over-produced by the CACM mechanism.

Formaldehyde concentrations (Fig. 4d), on the other hand, are close to observed mixing ratios and to those simulated by the RACM mechanism, supporting the hypothesis that it is over-production of isoprene peroxy radicals that is the cause of the elevated MVK-MCR concentrations in CACM. The elevated formaldehyde concentrations in CACM are the result of the lumping of all $\text{RO}_2^* + \text{HO}_2$ peroxides as a single proxy species that photolyses to produce formaldehyde, when in reality many of these would produce higher aldehydes. The diurnal profile of formaldehyde concentrations is still not a good match to measured concentrations with a marked over-production at night. This is likely due to the over-estimates of peroxy radical concentrations discussed above leading to excessive peroxy radical-peroxy radical reactions.

The changes implemented in the CACM gas-phase chemistry scheme, particularly the increase in the rate of $\text{RO}_2^* + \text{RO}_2^*$ reactions, had a substantial effect on the HO_x - NO_x species. Concentrations of NO_2 (Fig. 4e) and NO (Fig. 4f) now show typical diurnal profiles for each, with NO_2 depletion during the day and production from NO conversion overnight. Daytime NO_2 concentrations are in good agreement with those observed, but overnight recovery is too low with night-time concentrations around a factor of 2–3 below measured mixing ratios. In spite of the increased competition between $\text{RO}_2^* + \text{RO}_2^*$ and $\text{RO}_2^* + \text{NO}$ reactions, NO concentrations are still a factor of ~ 2 – 5 too low throughout the simulation, showing that there is still too much dependency on the NO reaction channel in the updated reaction scheme.

After the passage of the frontal system, ozone concentrations (Fig. 4g) are in close agreement with both measurements, and RACM and CACM0.0 simulated values, pointing again to the powerful buffering inherent in most atmospheric chemistry schemes. This raises concerns over whether such buffering genuinely occurs or whether current schemes are simply well-tuned to current conditions.

**FORest canopy
atmosphere transfer
(FORCAst) 1.0**K. Ashworth et al.

[Title Page](#)[Abstract](#)[Introduction](#)[Conclusions](#)[References](#)[Tables](#)[Figures](#)[Back](#)[Close](#)[Full Screen / Esc](#)[Printer-friendly Version](#)[Interactive Discussion](#)

FORest canopy atmosphere transfer (FORCAst) 1.0

K. Ashworth et al.

Title Page

Abstract

Introduction

Conclusions

References

Tables

Figures



Back

Close

Full Screen / Esc

Printer-friendly Version

Interactive Discussion



OH concentrations (Fig. 4h) are little affected by the alterations made to CACM0.0 indicating that it is the initial oxidation reactions and production via ozone that dominate the OH budget in current atmospheric chemistry schemes. However, mixing ratios are well below those observed, consistent with many field campaigns in low-NO_x environments (e.g. Ganzeveld et al., 2008; Stone et al., 2011; Wolfe et al., 2011; Lu et al., 2012). This shows the urgent need to fully update the CACM chemistry scheme (in particular the isoprene oxidation reactions) to reflect more recent understanding of reaction paths under such conditions.

CACM HO₂ concentrations (Fig. 4i) are substantially lower and HO₂* slightly higher (Fig. 4j) in comparison with observed levels of HO₂. In both cases, however, the changes implemented in CACM0.0 have brought CACM mixing ratios into much closer agreement with those simulated by RACM. The two schemes now display virtually identical diurnal profiles. The elevated HO₂* concentrations are most likely the result of the excessive peroxy radical production in CACM discussed above.

4.2.2 High-NO_x

Model output from CACM is compared to the RACM and CACM0.0 mechanisms for high-NO_x conditions in Fig. 6. For most species considered here, the alterations to the scheme make little difference to modelled mixing ratios. The biggest changes occur at night, with the increased RO₂* + RO₂* stimulating night-time chemistry. This results in greater overnight losses of the primary terpenoids (Fig. 6a and b) and increased MVK-MCR production (Fig. 6c) in particular. Although MVK-MCR concentrations remain well above those simulated in RACM, formaldehyde concentrations (Fig. 6d) are in much closer agreement. Concentrations of the HO_x-NO_x oxidant species are also brought more in line with the RACM output, with a marked increase in concentrations of both NO₂ (Fig. 6e) and NO (Fig. 6f) as the RO₂* and HO₂ reaction channels become competitive at relatively higher levels of NO_x.

HO₂ concentrations (Fig. 6i) are reduced to levels in line with those in RACM, but the most notable change is in the simulation of HO₂* (Fig. 6j). Not only are the abso-

lute levels in excellent agreement with RACM, the diurnal profile is now also a good match, with the tendency to over-accumulate isoprene peroxy radicals at night seen in CACM0.0 removed due to the increased night-time peroxy radical loss via the $RO_2^* + RO_2^*$ reactions.

4.3 Secondary organic aerosols

We applied the updated CACM gas-phase chemistry with the MPMPO aerosol module to simulate the production of SOA for the same two-day period under the observed low- NO_x conditions. For the simulations, primary organic aerosol (POA) concentration was set at a constant value of $0.5 \mu\text{g m}^{-3}$, consistent with simulated background concentrations during July for the region (Barsanti et al., 2013). Observed hourly submicron particle size distribution data for the simulation period, interpolated to 30 min intervals, were used to calculate volume-weight sedimentation velocities; aerosol aqueous phase pH was set at 4, consistent with the high sulfate to ammonium ratio measured at PROPHET during CABINEX (VanReken et al., 2015). Calculated hourly aerosol liquid water content (ALWC) data, also interpolated to 30 min intervals, based on hourly observed particle size distributions, CCN concentrations, and ambient relative humidity (see Supplement), were used as input to MPMPO. The lowest model layer was initialized with $2 \mu\text{g m}^{-3}$ of condensable gases split equally among the 99 condensable species; above the first layer, initial concentrations decreased exponentially with height (see Table S4).

Figure 7 shows the vertical and temporal profiles of predicted total (gas and aerosol phases) and aerosol-phase concentrations of condensable bVOC oxidation products. Time series of all condensable species and selected categories at 835 m (model layer 24) are shown in Fig. 8. In Fig. 7, the sum of gas- and aerosol-phase concentrations represents the total semi- and non-volatile material simulated by CACM. The oxidation of biogenic emissions produces up to $\sim 3 \mu\text{g m}^{-3}$ (or ~ 300 ppt) of condensable material from within the canopy to the top of the daytime boundary layer at ~ 1 km above the ground. The two-day CACM-MPMPO simulations indicate that below

FORest canopy atmosphere transfer (FORCAst) 1.0

K. Ashworth et al.

Title Page

Abstract

Introduction

Conclusions

References

Tables

Figures



Back

Close

Full Screen / Esc

Printer-friendly Version

Interactive Discussion



**FORest canopy
atmosphere transfer
(FORCAsT) 1.0**

K. Ashworth et al.

Title Page

Abstract

Introduction

Conclusions

References

Tables

Figures



Back

Close

Full Screen / Esc

Printer-friendly Version

Interactive Discussion



concentrations at UMBS during CABINEX. Submicron aerosol size distributions, CCN concentrations and water-soluble aerosol components, including water-soluble organic carbon (WSOC), sampled from the understory (6 m) of PROHET during CABINEX are reported in VanReken et al. (2015). During CABINEX WSOC concentrations averaged $2.5 \pm 2.9 \mu\text{g C g m}^{-3}$ (approximately $5.2 \pm 6.1 \mu\text{g m}^{-3}$ assuming carbon mass to total organic mass ratio of 2.1), much higher than Delia (2004) observed in 2001; however, concentrations were often below detection limits during CABINEX. The large standard deviation relative to the mean is due to the high temporal variability. For the two-day simulation period, anthropogenic influences were small and observed WSOC concentrations ranged from 0.4 to $6.4 \text{ C } \mu\text{g m}^{-3}$ (9 two-hour samples). The CACM-MPMPO predictions of less than $1 \mu\text{g m}^{-3}$ in the canopy are therefore an underestimation. One reason for the underestimation is that the model currently does not include explicit treatment of SOA from isoprene, despite the buildup of the S1 surrogate from MVK oxidation. Alternatively the over-prediction of temperatures at both the mid-day peak and at night, could result in a higher portion of condensable species remaining in the gas phase. Uncertainties in aqueous-phase pH and POA concentrations (associated with advection) may also contribute to the underestimation. Incorporation of an explicit treatment of SOA formation from isoprene and sesquiterpene oxidations and detailed evaluation with more comprehensive sets of gas, aerosol, and meteorological measurements, such as those from BEACHON (Ortega et al., 2014) and SOAS (e.g. Xu et al., 2015; Nguyen et al., 2014) are needed to elucidate the mechanism for SOA formation and to better understand measured-modeled discrepancies.

5 Conclusions

The 1-D CACHE canopy model (Forkel et al., 2006; Bryan et al., 2012) has been updated to include a modified version of the CACM gas-phase chemistry scheme (Griffin et al., 2002; Chen et al., 2005) and MPMPO aerosol partitioning mechanism (Griffin et al., 2003; Chen et al., 2005). In order to improve the performance of CACM for

**FORest canopy
atmosphere transfer
(FORCAsT) 1.0**

K. Ashworth et al.

[Title Page](#)[Abstract](#)[Introduction](#)[Conclusions](#)[References](#)[Tables](#)[Figures](#)[Back](#)[Close](#)[Full Screen / Esc](#)[Printer-friendly Version](#)[Interactive Discussion](#)

low NO_x conditions the peroxy radical and organic nitrate reactions in the gas-phase chemistry have been updated. Given the substantial NO_x emissions decreases due to implementation of emissions control strategies in many mid-latitude areas it will become increasingly important in future applications to address lower NO_x scenarios in many rural and even urban areas traditionally considered to be high- NO_x regions.

This new model, FORCAsT 1.0, is one of the few canopy exchange models that incorporate both the gas-phase oxidation of VOCs and the production of condensable products that can lead to SOA formation. Thus FORCAsT represents a substantial step forward in canopy-atmosphere exchange modeling, with the potential to significantly enhance our understanding of the processes involved, their relative importance under different regimes, and the ability to validate our knowledge against site-specific measurement data. Insights gained from the application of FORCAsT can be used to improve 3-D models of regional and global atmospheric chemistry and climate.

Previous evaluation of model performance at the UMBS field station for the CABINEX field campaign (Bryan et al., 2012) demonstrated that its predecessor CACHE was able to reproduce environmental conditions at the site. We show here that FORCAsT also effectively reproduces mixing ratios of many key species associated with the oxidation of bVOCs. However, in line with many other box and column models (e.g. Ganzeveld et al., 2008), FORCAsT displays a tendency to accumulate the products of VOC oxidation, in particular methyl vinyl ketone and methacrolein, and formaldehyde, most likely as a result of over-production of peroxy radicals from isoprene oxidation in particular. Discrepancies between observed and simulated concentrations of the primary HO_x - NO_x oxidants also suggest that further improvement is required in the representation of gas-phase reaction pathways under low- NO_x conditions to better capture the degradation of VOCs in such environments. However, the sensitivity studies and chemistry mechanism updates included here have provided valuable insight into the importance of peroxy-peroxy radical reactions, production and loss of organic nitrates, and night-time chemistry in controlling the oxidative capacity of the atmosphere within and above forest ecosystems.

**FORest canopy
atmosphere transfer
(FORCAsT) 1.0**

K. Ashworth et al.

[Title Page](#)[Abstract](#)[Introduction](#)[Conclusions](#)[References](#)[Tables](#)[Figures](#)[Back](#)[Close](#)[Full Screen / Esc](#)[Printer-friendly Version](#)[Interactive Discussion](#)

The difficulty displayed by the CACM chemistry mechanism in reproducing observed concentrations of the HO_x-NO_x species in particular, clearly demonstrates that our lack of understanding of the oxidation reactions of bVOCs, especially isoprene, are not just an issue for remote pristine regions in the Southern Hemisphere. Recent legislation to improve air quality by reducing NO_x emissions in the northern mid-latitudes, means that many rural locations in this region now have sufficiently high VOC : NO_x ratios that VOC oxidation in these locations will also follow what has previously been thought of as “low NO_x chemistry” routes. This study points to the urgent need to constrain concentrations of key short-lived radical species such as organic peroxy radicals in and above forest ecosystems, and to elucidate the mechanisms and processes governing their production and loss. Such insight can be improved through fully integrated field measurement-modelling campaigns and through the establishment of long-term comprehensive measurement networks and datasets.

Future development work for FORCAsT includes additional improvements in its simulation of gas-phase chemistry and SOA formation under low-NO_x conditions. This will include updating the oxidation reactions of bVOCs, in particular isoprene, to reflect the latest advances in our understanding of these pathways and their importance in the formation of SOA, such as through the isoprene epoxide pathway. SOA formation from MBO (2-methyl-3-buten-2-ol) and sesquiterpenes will also be added. FORCAsT will also be tested against field and long-term gas-phase and aerosol campaign measurements from many more sites under a spectrum of NO_x concentrations.

Code availability

FORCAsT 1.0 is available by request to the corresponding author. Users of the code will be asked to cite this work, and include appropriate references to CACHE, CUPID and CACM-MPMPO, in publications based on its application.

Acknowledgements. This material is based upon work supported by the National Science Foundation under Grant No. AGS 1242203.

References

- Atkinson, R. and Arey, J.: Gas-phase tropospheric chemistry of biogenic volatile organic compounds: a review, *Atmos. Environ.*, 37, 197–219, doi:10.1016/S1352-2310(03)00391-1, 2003.
- Baldocchi, D.: A Multi-layer model for estimating sulfur dioxide deposition to a deciduous oak forest canopy, *Atmos. Environ.*, 22, 869–884, 1988.
- Barsanti, K. C., Carlton, A. G., and Chung, S. H.: Analyzing experimental data and model parameters: implications for predictions of SOA using chemical transport models, *Atmos. Chem. Phys.*, 13, 12073–12088, doi:10.5194/acp-13-12073-2013, 2013.
- Beaver, M. R., Clair, J. M. St., Paulot, F., Spencer, K. M., Crouse, J. D., LaFranchi, B. W., Min, K. E., Pusede, S. E., Wooldridge, P. J., Schade, G. W., Park, C., Cohen, R. C., and Wennberg, P. O.: Importance of biogenic precursors to the budget of organic nitrates: observations of multifunctional organic nitrates by CIMS and TD-LIF during BEARPEX 2009, *Atmos. Chem. Phys.*, 12, 5773–5785, doi:10.5194/acp-12-5773-2012, 2012.
- Blackadar, A. K.: Vertical distribution of wind and turbulent exchange in a neutral atmosphere, *J. Geophys. Res.*, 67, 3095–3102, doi:10.1029/JZ067i008p03095, 1962.
- Boy, M., Sogachev, A., Lauros, J., Zhou, L., Guenther, A., and Smolander, S.: SOSA – a new model to simulate the concentrations of organic vapours and sulphuric acid inside the ABL – Part 1: Model description and initial evaluation, *Atmos. Chem. Phys.*, 11, 43–51, doi:10.5194/acp-11-43-2011, 2011.
- Brown, S. S., deGouw, J. A., Warneke, C., Ryerson, T. B., Dubé, W. P., Atlas, E., Weber, R. J., Peltier, R. E., Neuman, J. A., Roberts, J. M., Swanson, A., Flocke, F., McKeen, S. A., Brioude, J., Sommariva, R., Trainer, M., Fehsenfeld, F. C., and Ravishankara, A. R.: Nocturnal isoprene oxidation over the Northeast United States in summer and its impact on

FORest canopy atmosphere transfer (FORCAst) 1.0

K. Ashworth et al.

Title Page

Abstract

Introduction

Conclusions

References

Tables

Figures



Back

Close

Full Screen / Esc

Printer-friendly Version

Interactive Discussion



**FORest canopy
atmosphere transfer
(FORCAst) 1.0**

K. Ashworth et al.

[Title Page](#)[Abstract](#)[Introduction](#)[Conclusions](#)[References](#)[Tables](#)[Figures](#)[Back](#)[Close](#)[Full Screen / Esc](#)[Printer-friendly Version](#)[Interactive Discussion](#)

reactive nitrogen partitioning and secondary organic aerosol, *Atmos. Chem. Phys.*, 9, 3027–3042, doi:10.5194/acp-9-3027-2009, 2009.

Browne, E. C. and Cohen, R. C.: Effects of biogenic nitrate chemistry on the NO_x lifetime in remote continental regions, *Atmos. Chem. Phys.*, 12, 11917–11932, doi:10.5194/acp-12-11917-2012, 2012.

Bryan, A. M., Bertman, S. B., Carroll, M. A., Dusanter, S., Edwards, G. D., Forkel, R., Griffith, S., Guenther, A. B., Hansen, R. F., Helmig, D., Jobson, B. T., Keutsch, F. N., Lefer, B. L., Pressley, S. N., Shepson, P. B., Stevens, P. S., and Steiner, A. L.: In-canopy gas-phase chemistry during CABINEX 2009: sensitivity of a 1-D canopy model to vertical mixing and isoprene chemistry, *Atmos. Chem. Phys.*, 12, 8829–8849, doi:10.5194/acp-12-8829-2012, 2012.

Carroll, M. A., Bertman, S. B., and Shepson, P. B.: Overview of the Program for Research on Oxidants: PHotochemistry, Emissions, and Transport (PROPHET) summer 1998 measurements intensive, *J. Geophys. Res.*, 106, 24275–24288, 2001.

Chen, J. and Griffin, R. J.: Modeling secondary organic aerosol formation from oxidation of α -pinene, β -pinene, and *d*-limonene, *Atmos. Environ.*, 39, 7731–7744, doi:10.1016/j.atmosenv.2005.05.049, 2005.

Chen, J., Mao, H., Talbot, R. W., and Griffin, R. J.: Application of the CACM and MPMPO modules using the CMAQ model for the eastern United States, *J. Geophys. Res.*, 111, D23S25, doi:10.1029/2006JD007603, doi:200610.1029/2006JD007603, 2006.

Chen, J., Griffin, R. J., Grini, A., and Tulet, P.: Modeling secondary organic aerosol formation through cloud processing of organic compounds, *Atmos. Chem. Phys.*, 7, 5343–5355, doi:10.5194/acp-7-5343-2007, 2007.

Chen, J. J., Ying, Q., and Kleeman, M. J.: Source apportionment of wintertime secondary organic aerosol during the California regional PM₁₀/PM_{2.5} air quality study, *Atmos. Environ.*, 44, 1331–1340, doi:10.1016/j.atmosenv.2009.07.010, 2010.

Delia, A.: Real-Time Measurements of Non-Refractory Particle Composition and Interactions at Rural and Semi-Rural Sites, PhD Thesis, University of Colorado-Boulder, 2004.

Emmerson, K. M. and Evans, M. J.: Comparison of tropospheric gas-phase chemistry schemes for use within global models, *Atmos. Chem. Phys.*, 9, 1831–1845, doi:10.5194/acp-9-1831-2009, 2009.

Forkel, R., Klemm, O., Graus, M., Rappenglück, B., Stockwell, W. R., Grabmer, W., Held, A., Hansel, A., and Steinbrecher, R.: Trace gas exchange and gas phase chemistry in a Norway

FORest canopy atmosphere transfer (FORCAsT) 1.0

K. Ashworth et al.

Title Page

Abstract

Introduction

Conclusions

References

Tables

Figures



Back

Close

Full Screen / Esc

Printer-friendly Version

Interactive Discussion



- spruce forest: a study with a coupled 1-dimensional canopy atmospheric chemistry emission model, *Atmos. Environ.*, 40, 28–42, doi:10.1016/j.atmosenv.2005.11.070, 2006.
- Fredenslund, A., Gmehling, J., and Rasmussen, P.: Vapor–Liquid Equilibrium Using UNIFAC, Elsevier Sci., New York, 1977.
- 5 Friedlingston, P. and Prentice, I. C.: Carbon-climate feedbacks: a review of model and observation based estimates, *Curr. Opin. Environ. Sustainability*, 2, 251–257, 2010.
- Fuchs, H., Bohn, B., Hofzumahaus, A., Holland, F., Lu, K. D., Nehr, S., Rohrer, F., and Wahner, A.: Detection of HO₂ by laser-induced fluorescence: calibration and interferences from RO₂ radicals, *Atmos. Meas. Tech.*, 4, 1209–1225, doi:10.5194/amt-4-1209-2011, 2011.
- 10 Ganzeveld, L. N., Lelieveld, J., Dentener, F. J., Krol, M. C., and Roelofs, G. J.: Atmosphere–biosphere trace gas exchanges simulated with a single-column model, *J. Geophys. Res.*, 107, 4297, doi:10.1029/2001JD000684, 2002.
- Ganzeveld, L., Eerdeken, G., Feig, G., Fischer, H., Harder, H., Königstedt, R., Kubistin, D., Martinez, M., Meixner, F. X., Scheeren, H. A., Sinha, V., Taraborrelli, D., Williams, J., Vilà-Guerau de Arellano, J., and Lelieveld, J.: Surface and boundary layer exchanges of volatile organic compounds, nitrogen oxides and ozone during the GABRIEL campaign, *Atmos. Chem. Phys.*, 8, 6223–6243, doi:10.5194/acp-8-6223-2008, 2008.
- 15 Gao, W., Wesely, M. L., and Doskey, P. V.: Numerical modeling of the turbulent diffusion and chemistry of NO_x, O₃, isoprene, and other reactive trace gases in and above a forest canopy, *J. Geophys. Res.*, 98, 18339–18353, doi:10.1029/93JD01862, 1993.
- Geiger, H., Barnes, I., Bejan, I., Benter, T., and Spittler, M.: The tropospheric degradation of isoprene: an updated module for the regional atmospheric chemistry mechanism, *Atmos. Environ.*, 37, 1503–1519, 2003.
- Goel, N. S. and Strebel, D. E.: Simple beta distribution representation of leaf orientation in vegetation canopies, *Agron. J.*, 76, 800–802, 1984.
- 25 Grace, J., Cox, P., and Meir, P.: The influence of terrestrial ecosystems on climate, *Trends Ecol. Evol.*, 21, 254–260, 2006.
- Griffin, R. J., Dabdub, D., and Seinfeld, J. H.: Secondary organic aerosol 1. Atmospheric chemical mechanism for production of molecular constituents, *J. Geophys. Res.*, 107, 4332, doi:10.1029/2001JD000541, 2002.
- 30 Griffin, R. J., Nguyen, K., Dabdub, D., and Seinfeld, J. H.: A coupled hydrophobic-hydrophilic model for predicting secondary organic aerosol formation, *J. Atmos. Chem.*, 44, 171–190, 2003.

**FORest canopy
atmosphere transfer
(FORCAst) 1.0**

K. Ashworth et al.

[Title Page](#)[Abstract](#)[Introduction](#)[Conclusions](#)[References](#)[Tables](#)[Figures](#)[Back](#)[Close](#)[Full Screen / Esc](#)[Printer-friendly Version](#)[Interactive Discussion](#)

Griffin, R. J., Dabdub, D., and Seinfeld, J. H.: Development and initial evaluation of a dynamic species-resolved model for gas phase chemistry and size-resolved gas/particle partitioning associated with secondary organic aerosol formation, *J. Geophys. Res.*, 110, D05304, doi:10.1029/2004JD005219, 2005.

5 Griffith, S. M., Hansen, R. F., Dusanter, S., Stevens, P. S., Alaghmand, M., Bertman, S. B., Carroll, M. A., Erickson, M., Galloway, M., Grossberg, N., Hottle, J., Hou, J., Jobson, B. T., Kammrath, A., Keutsch, F. N., Lefer, B. L., Mielke, L. H., O'Brien, A., Shepson, P. B., Thurlow, M., Wallace, W., Zhang, N., and Zhou, X. L.: OH and HO₂ radical chemistry during PROPHET 2008 and CABINEX 2009 – Part 1: Measurements and model comparison, *Atmos. Chem. Phys.*, 13, 5403–5423, doi:10.5194/acp-13-5403-2013, 2013.

10 Guenther, A., Hewitt, C. N., Erickson, D., Fall, R., Geron, C., Graedel, T., Harley, P., Klinger, L., Lerdau, M., McKay, W. A., Pierce, T., Scholes, B., Steinbrecher, R., Tallamraju, R., Taylor, J., and Zimmerman, P.: A global model of natural volatile organic compound emissions, *J. Geophys. Res.*, 100, 8873–8892, doi:10.1029/94JD02950, 1995.

15 Harris, J. C. and Hayes, M. J.: Acid dissociation constant, in: *Handbook of Chemical Property Estimation and Methods: Environmental Behavior of Organic Compounds*, edited by: Lyman, W. J., Reehl, W. F., and Rosenblatt, D. H., McGraw-Hill, New York, 1982.

Jenkin, M. E., Saunders, S. M., and Pilling, M. J.: The tropospheric degradation of volatile organic compounds: a protocol for mechanism development, *Atmos. Environ.*, 31, 81–104, doi:10.1016/S1352-2310(96)00105-7, 1997.

20 Kanawade, V. P., Jobson, B. T., Guenther, A. B., Erupe, M. E., Pressley, S. N., Tripathi, S. N., and Lee, S.-H.: Isoprene suppression of new particle formation in a mixed deciduous forest, *Atmos. Chem. Phys.*, 11, 6013–6027, doi:10.5194/acp-11-6013-2011, 2011.

Karl, T., Harley, P., Emmons, L., Thornton, B., Guenther, A., Basu, C., Turnipseed, A., and Jardine, K.: Efficient atmospheric cleansing of oxidized organic trace gases by vegetation, *Science*, 330, 6005, 816–819, doi:10.1126/science.1192534, 2010.

25 Kim, S., Guenther, A., Karl, T., and Greenberg, J.: Contributions of primary and secondary biogenic VOC to total OH reactivity during the CABINEX (Community Atmosphere-Biosphere INTERactions Experiments)-09 field campaign, *Atmos. Chem. Phys.*, 11, 8613–8623, doi:10.5194/acp-11-8613-2011, 2011.

30 Laothawornkikul, J., Taylor, J. E., Paul, N. D., and Hewitt, C. N.: Biogenic volatile organic compounds in the Earth system, *New Phytol.*, 183, 27–51, doi:10.1111/j.1469-8137.2009.02859.x, 2009.

**FORest canopy
atmosphere transfer
(FORCAst) 1.0**

K. Ashworth et al.

Title Page

Abstract

Introduction

Conclusions

References

Tables

Figures



Back

Close

Full Screen / Esc

Printer-friendly Version

Interactive Discussion



- Lelieveld, J., Butler, T. M., Crowley, J. N., Dillon, T. J., Fischer, H., Ganzeveld, L., Harder, H., Lawrence, M. G., Martinez, M., Taraborrelli, D., and Williams, J.: Atmospheric oxidation capacity sustained by a tropical forest, *Nature*, 452, 737–740, doi:10.1038/nature06870, 2008.
- Lu, K. D., Rohrer, F., Holland, F., Fuchs, H., Bohn, B., Brauers, T., Chang, C. C., Häseler, R., Hu, M., Kita, K., Kondo, Y., Li, X., Lou, S. R., Nehr, S., Shao, M., Zeng, L. M., Wahner, A., Zhang, Y. H., and Hofzumahaus, A.: Observation and modelling of OH and HO₂ concentrations in the Pearl River Delta 2006: a missing OH source in a VOC rich atmosphere, *Atmos. Chem. Phys.*, 12, 1541–1569, doi:10.5194/acp-12-1541-2012, 2012.
- Mellouki, A., Wallington, T. J., and Chen, J.: Atmospheric chemistry of oxygenated volatile organic compounds: impacts on air quality and climate, *Chem. Rev.*, 115, 3984–4014, doi:10.1021/cr500549n, 2015.
- Meng, Z. Y., Dabdub, D., and Seinfeld, J. H.: Size-resolved and chemically resolved model of atmospheric aerosol dynamics, *J. Geophys. Res.*, 103, 3419–3435, doi:10.1029/97JD02796, 1998.
- Meyers, T. P. and Baldocchi, D. D.: A comparison of models for deriving dry deposition fluxes of O₃ and SO₂ to a forest canopy, *Tellus B*, 40, 270–284, doi:10.1111/j.1600-0889.1988.tb00297.x, 1988.
- Miyoshi, A., Hatakeyama, S., and Washida, N.: OH radical-initiated photooxidation of isoprene: an estimate of global CO production, *J. Geophys. Res.*, 99, 18779–18787, doi:10.1029/94JD01334, 1994.
- Müller, J.-F., Peeters, J., and Stavrou, T.: Fast photolysis of carbonyl nitrates from isoprene, *Atmos. Chem. Phys.*, 14, 2497–2508, doi:10.5194/acp-14-2497-2014, 2014.
- Nguyen, T. K. V., Petters, M. D., Suda, S. R., Guo, H., Weber, R. J., and Carlton, A. G.: Trends in particle-phase liquid water during the Southern Oxidant and Aerosol Study, *Atmos. Chem. Phys.*, 14, 10911–10930, doi:10.5194/acp-14-10911-2014, 2014.
- Norman, J. M.: Modeling the complete crop canopy, in: *Modification of the Aerial Environment of Plants*, edited by: Barfield, B. J. and Gerber, J. F., ASAE Monogr. Am. Soc. Agric. Eng., St. Joseph, M I., 249–277, 1979.
- Norman, J. M. and Campbell, G. S.: Application of a plant-environment model to problems in irrigation, in: *Advances in irrigation*, Vol. II., edited by: Hillel, D. I., Academic Press, New York, 155–188, 1983.
- Ortega, J., Turnipseed, A., Guenther, A. B., Karl, T. G., Day, D. A., Gochis, D., Huffman, J. A., Prenni, A. J., Levin, E. J. T., Kreidenweis, S. M., DeMott, P. J., Tobo, Y., Patton, E. G.,

**FORest canopy
atmosphere transfer
(FORCAst) 1.0**

K. Ashworth et al.

Title Page

Abstract

Introduction

Conclusions

References

Tables

Figures



Back

Close

Full Screen / Esc

Printer-friendly Version

Interactive Discussion



Hodzic, A., Cui, Y. Y., Harley, P. C., Hornbrook, R. S., Apel, E. C., Monson, R. K., Eller, A. S. D., Greenberg, J. P., Barth, M. C., Campuzano-Jost, P., Palm, B. B., Jimenez, J. L., Aiken, A. C., Dubey, M. K., Geron, C., Offenberg, J., Ryan, M. G., Fornwalt, P. J., Pryor, S. C., Keutsch, F. N., DiGangi, J. P., Chan, A. W. H., Goldstein, A. H., Wolfe, G. M., Kim, S., Kaser, L., Schnitzhofer, R., Hansel, A., Cantrell, C. A., Mauldin, R. L., and Smith, J. N.: Overview of the Manitou Experimental Forest Observatory: site description and selected science results from 2008 to 2013, *Atmos. Chem. Phys.*, 14, 6345–6367, doi:10.5194/acp-14-6345-2014, 2014.

Pankow, J. F.: An absorptive model of gas-particle partitioning of organic compounds in the atmosphere, *Atmos. Environ.*, 28, 185–188, doi:10.1016/1352-2310(94)90093-0, 1994.

Pankow, J. F., Seinfeld, J. H., Asher, W. E., and Erdakos, G. B.: Modeling the formation of secondary organic aerosol, 1, Application of theoretical principles to measurements obtained in the α -pinene-, β -pinene-, sabinene-, $\Delta(3)$ -carene-, and cyclohexene-ozone systems, *Environ. Sci. Technol.*, 35, 1164–1172, doi:10.1021/es001321d, 2001.

Paulot, F., Crounse, J. D., Kjaergaard, H. G., Kroll, J. H., Seinfeld, J. H., and Wennberg, P. O.: Isoprene photooxidation: new insights into the production of acids and organic nitrates, *Atmos. Chem. Phys.*, 9, 1479–1501, doi:10.5194/acp-9-1479-2009, 2009.

Peeters, J., Nguyen, T. L., and Vereecken, L.: HO_x radical regeneration in the oxidation of isoprene, *Phys. Chem. Chem. Phys.*, 11, 5935–5939, doi:10.1039/b908511d, 2009.

Perring, A. E., Pusede, S. E., and Cohen, R. C.: An observational perspective on the atmospheric impacts of alkyl and multifunctional nitrates on ozone and secondary organic aerosol, *Chem. Rev.*, 113, 5848–5870, doi:10.1021/cr300520x, 2013.

Pongratz, J., Reick, C. H., Raddatz, T., and Claussen, M.: Biogeophysical vs. biogeochemical climate response to historical anthropogenic land cover change, *Geophys. Res. Lett.*, 37, L08702, doi:10.1029/2010GL043010, 2010.

Pöschl, Ü., von Kuhlmann, R., Poisson, N., and Crutzen, P. J.: Development and intercomparison of condensed isoprene oxidation mechanisms for global atmospheric modeling, *J. Atmos. Chem.*, 37, 29–52, doi:10.1023/A:1006391009798, 2000.

Pun, B. K., Griffin, R. J., Seigneur, C., and Seinfeld, J. H.: Secondary organic aerosol 2, thermodynamic model for gas/particle partitioning of molecular constituents, *J. Geophys. Res.*, 107, 4333, doi:10.1029/2001JD000542, 2002.

**FORest canopy
atmosphere transfer
(FORCAst) 1.0**

K. Ashworth et al.

[Title Page](#)[Abstract](#)[Introduction](#)[Conclusions](#)[References](#)[Tables](#)[Figures](#)[Back](#)[Close](#)[Full Screen / Esc](#)[Printer-friendly Version](#)[Interactive Discussion](#)

- Sandu, A. and Sander, R.: Technical note: Simulating chemical systems in Fortran90 and Matlab with the Kinetic PreProcessor KPP-2.1, *Atmos. Chem. Phys.*, 6, 187–195, doi:10.5194/acp-6-187-2006, 2006.
- 5 Saunders, S. M., Jenkin, M. E., Derwent, R. G., and Pilling, M. J.: Protocol for the development of the Master Chemical Mechanism, MCM v3 (Part A): tropospheric degradation of non-aromatic volatile organic compounds, *Atmos. Chem. Phys.*, 3, 161–180, doi:10.5194/acp-3-161-2003, 2003.
- Saxena, P. and Hildemann, L. M.: Water absorption by organics: survey of laboratory evidence and evaluation of UNIFAC for estimating water activity, *Environ. Sci. Technol.*, 31, 3318–3324, doi:10.1021/es9703638, 1997.
- 10 Schwarzenbach, R. P., Gschwend, P. M., and Imboden, D. M.: *Environmental Organic Chemistry*, John Wiley, New York, 1993.
- Seinfeld, J. H., Erdakos, G. B., Asher, W. E., and Pankow, J. F.: Modeling the formation of secondary organic aerosol (SOA), 2, the predicted effects of relative humidity on aerosol formation in the alpha-pinene-, beta-pinene-, sabinene-, Delta(3)-Carene-, and cyclohexene-ozone systems, *Environ. Sci. Technol.*, 35, 1806–1817, doi:10.1021/es001765+, 2001.
- 15 Smith, J. M. and Van Ness, H. C.: *Introduction to Chemical Engineering Thermodynamics*, McGraw-Hill, Inc., New York., 1987.
- Steinbrecher, R., Hauff, K., Hakola, H., and Rössler, J.: A revised parameterisation for emission modelling of isoprenoids for boreal plants, in: *Biogenic VOC Emissions and Photochemistry in the Boreal Regions of Europe – Biphorep*, in: *Air pollution research report, no. 70*, edited by: Laurila, T. and Lindfors, V., Commission of the European Communities, EUR 18910 E N. EC, Brussels, 29–43, 1999.
- 20 Steiner, A. L., Pressley, S. N., Botros, A., Jones, E., Chung, S. H., and Edburg, S. L.: Analysis of coherent structures and atmosphere-canopy coupling strength during the CABINEX field campaign, *Atmos. Chem. Phys.*, 11, 11921–11936, doi:10.5194/acp-11-11921-2011, 2011.
- Stockwell, W. R., Kirchner, F., Kuhn, M., and Seefeld, S.: A new mechanism for regional atmospheric chemistry modeling, *J. Geophys. Res.*, 102, 25847–25879, doi:10.1029/97JD00849, 1997.
- 30 Stone, D., Evans, M. J., Edwards, P. M., Commane, R., Ingham, T., Rickard, A. R., Brookes, D. M., Hopkins, J., Leigh, R. J., Lewis, A. C., Monks, P. S., Oram, D., Reeves, C. E., Stewart, D., and Heard, D. E.: Isoprene oxidation mechanisms: measurements and modelling

FORest canopy atmosphere transfer (FORCAst) 1.0

K. Ashworth et al.

Title Page

Abstract

Introduction

Conclusions

References

Tables

Figures



Back

Close

Full Screen / Esc

Printer-friendly Version

Interactive Discussion



- of OH and HO₂ over a South-East Asian tropical rainforest during the OP3 field campaign, *Atmos. Chem. Phys.*, 11, 6749–6771, doi:10.5194/acp-11-6749-2011, 2011.
- Strebel, D. E., Goel, N. S., and Ronson, K. J.: Two-dimensional leaf orientation distributions, *IEEE T. Geosci. Remote*, GE-23, 640–647, 1985.
- 5 Stroud, C., Makar, P., Karl, T., Guenther, A., Geron, C., Turnipseed, A., Nemitz, E., Baker, B., Potosnak, M., and Fuentes, J. D.: Role of canopy-scale photochemistry in modifying biogenic-atmosphere exchange of reactive terpene species: results from the CELTIC field study, *J. Geophys. Res.*, 110, D17303, doi:10.1029/2005JD005775, 2005.
- Sumner, A. L., Shepson, P. B., Couch, T. L., Thornberry, T., Carroll, M. A., Sillman, S., Pip-
 10 pin, M., Bertman, S., Tan, D., Faloon, I., Brune, W., Young, V., Cooper, O., Moody, J., and Stockwell, W.: A study of formaldehyde chemistry above a forest canopy, *J. Geophys. Res.*, 106, 24387–24405, doi:10.1029/2000JD900761, 2001.
- Suzuki, T., Ohtaguchi, K., and Koide, K.: Application of principal components analysis to calculate Henry's constant from molecular structure, *Comput. Chem.*, 16, 41–52, 1992.
- 15 VanReken, T. M., Mwaniki, G. R., Wallace, H. W., Pressley, S. N., Erickson, M. H., Jobson, B. T., and Lamb, B. K.: Influence of air mass origin on aerosol properties at a remote Michigan forest site, *Atmos. Environ.*, 107, 35–43, doi:10.1016/j.atmosenv.2015.02.027, 2015.
- Wesely, M. L.: Parameterization of surface resistances to gaseous dry deposition in regional-scale numerical-models, *Atmos. Environ.*, 23, 1293–1304, doi:10.1016/0004-
 20 6981(89)90153-4, 1989.
- Whalley, L., Stone, D., and Heard, D.: New Insights into the Tropospheric Oxidation of Isoprene: Combining Field Measurements, Laboratory Studies, Chemical Modelling and Quantum Theory, in: *Atmospheric and Aerosol Chemistry, Topics in Current Chemistry Series*, edited by: McNeill, V. F. and Ariya, P. A., Springer-Verlag Berlin, Berlin, Germany, 339, 55–95, 2014.
- 25 Wild, O.: Modelling the global tropospheric ozone budget: exploring the variability in current models, *Atmos. Chem. Phys.*, 7, 2643–2660, doi:10.5194/acp-7-2643-2007, 2007.
- Williams, J., Fuentes, J., Hofzumahaus, A., and Abbatt, J. (Eds.): *Community Atmosphere-Biosphere Interactions Experiment 2009 (CABINEX), Special Issue*, *Atmos. Chem. Phys.*, http://www.atmos-chem-phys.net/special_issue234.html, 2011.
- 30 Wolfe, G. M. and Thornton, J. A.: The Chemistry of Atmosphere-Forest Exchange (CAFE) Model – Part 1: Model description and characterization, *Atmos. Chem. Phys.*, 11, 77–101, doi:10.5194/acp-11-77-2011, 2011.

**FORest canopy
atmosphere transfer
(FORCAst) 1.0**

K. Ashworth et al.

Title Page

Abstract

Introduction

Conclusions

References

Tables

Figures



Back

Close

Full Screen / Esc

Printer-friendly Version

Interactive Discussion



Wolfe, G. M., Thornton, J. A., Bouvier-Brown, N. C., Goldstein, A. H., Park, J.-H., McKay, M., Matross, D. M., Mao, J., Brune, W. H., LaFranchi, B. W., Browne, E. C., Min, K.-E., Wooldridge, P. J., Cohen, R. C., Crounse, J. D., Faloona, I. C., Gilman, J. B., Kuster, W. C., de Gouw, J. A., Huisman, A., and Keutsch, F. N.: The Chemistry of Atmosphere-Forest Exchange (CAFE) Model – Part 2: Application to BEARPEX-2007 observations, *Atmos. Chem. Phys.*, 11, 1269–1294, doi:10.5194/acp-11-1269-2011, 2011.

Wolfe, G. M., Cantrell, C., Kim, S., Mauldin III, R. L., Karl, T., Harley, P., Turnipseed, A., Zheng, W., Flocke, F., Apel, E. C., Hornbrook, R. S., Hall, S. R., Ullmann, K., Henry, S. B., DiGangi, J. P., Boyle, E. S., Kaser, L., Schnitzhofer, R., Hansel, A., Graus, M., Nakashima, Y., Kajii, Y., Guenther, A., and Keutsch, F. N.: Missing peroxy radical sources within a summer-time ponderosa pine forest, *Atmos. Chem. Phys.*, 14, 4715–4732, doi:10.5194/acp-14-4715-2014, 2014.

Xu, L., Guo, H., Boyd, C. M., Klein, M., Bougiatioti, A., Cerully, K. M., Hite, J. R., Isaacman-VanWertz, G., Kreisberg, N. M., Knote, C., Olson, K., Koss, A., Goldstein, A. H., Hering, S. V., de Gouw, J., Baumann, K., Lee, S.-H., Nenes, A., Weber, R. J., and Ng, N. L.: Effects of anthropogenic emissions on aerosol formation from isoprene and monoterpenes in the south-eastern United States, *P. Natl. Acad. Sci. USA*, 112, 37–42, 2015.

Young, P. J., Archibald, A. T., Bowman, K. W., Lamarque, J.-F., Naik, V., Stevenson, D. S., Tilmes, S., Voulgarakis, A., Wild, O., Bergmann, D., Cameron-Smith, P., Cionni, I., Collins, W. J., Dalsøren, S. B., Doherty, R. M., Eyring, V., Faluvegi, G., Horowitz, L. W., Josse, B., Lee, Y. H., MacKenzie, I. A., Nagashima, T., Plummer, D. A., Righi, M., Rumbold, S. T., Skeie, R. B., Shindell, D. T., Stroe, S. A., Sudo, K., Szopa, S., and Zeng, G.: Pre-industrial to end 21st century projections of tropospheric ozone from the Atmospheric Chemistry and Climate Model Intercomparison Project (ACCMIP), *Atmos. Chem. Phys.*, 13, 2063–2090, doi:10.5194/acp-13-2063-2013, 2013.

Zhang, N., Zhou, X., Bertman, S., Tang, D., Alaghmand, M., Shepson, P. B., and Carroll, M. A.: Measurements of ambient HONO concentrations and vertical HONO flux above a northern Michigan forest canopy, *Atmos. Chem. Phys.*, 12, 8285–8296, doi:10.5194/acp-12-8285-2012, 2012.

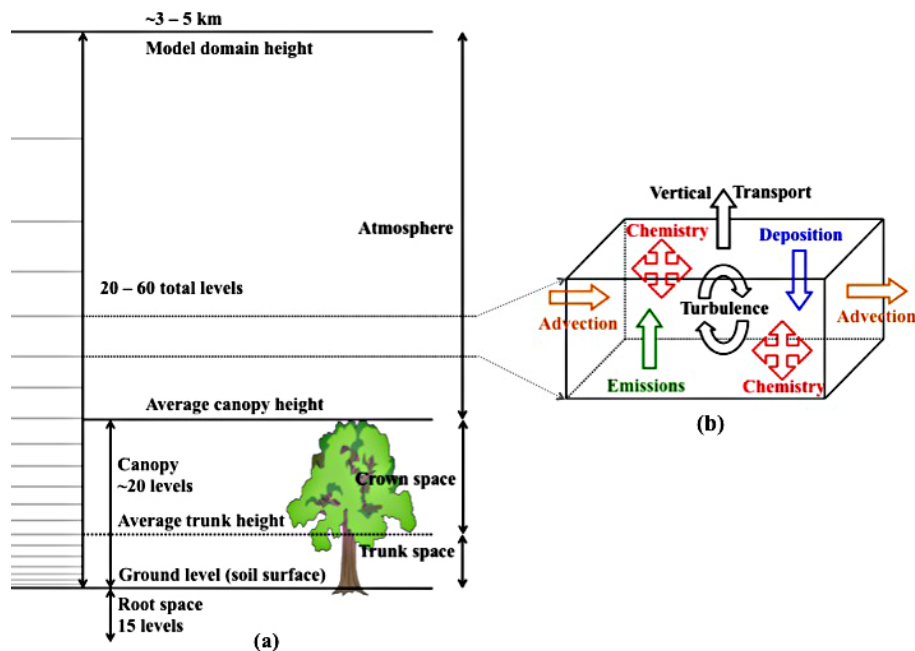


Figure 1. (a) A schematic of the FORCAst column model. Each level within the column is a box model (b) incorporating the processes involved in canopy-atmosphere exchange of energy and mass appropriate for that level.

FORest canopy atmosphere transfer (FORcAsT) 1.0

K. Ashworth et al.

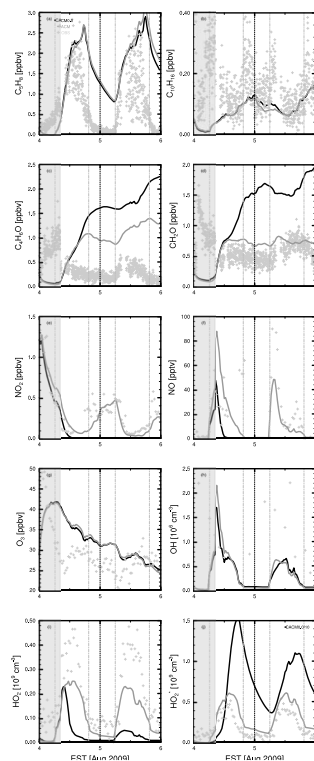


Figure 2. Concentrations of **(a)** isoprene, **(b)** summed monoterpenes, **(c)** MVK-MCR, **(d)** formaldehyde, **(e)** NO₂, **(f)** NO, **(g)** ozone, **(h)** OH, **(i)** HO₂, and **(j)** HO₂^{*} for 04–05 August 2009 at the top of the flux tower (corresponding to 36.94 m for model output data and 34 m for measurements). Model data from CACM0.0 is shown in black, and RACM in grey; measurement data are shown by crosses. Note the scale for CACM0.0 in **(j)**.

Title Page

Abstract

Introduction

Conclusions

References

Tables

Figures

◀

▶

◀

▶

Back

Close

Full Screen / Esc

Printer-friendly Version

Interactive Discussion



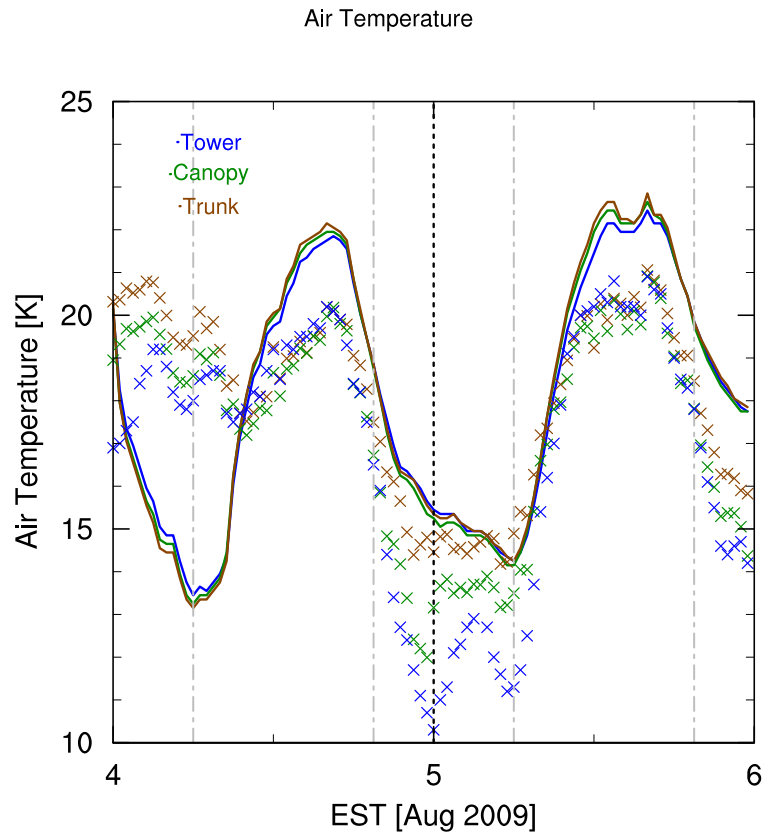


Figure 3. Air temperatures at the trunk height (6 m), canopy top (20.4 m for observations and 19.47 m for FORCASt output) and tower top (34 m for observations and 36.94 m for FORCASt output).

Title Page

Abstract Introduction

Conclusions References

Tables Figures

◀ ▶

◀ ▶

Back Close

Full Screen / Esc

Printer-friendly Version

Interactive Discussion



FORest canopy atmosphere transfer (FORcAsT) 1.0

K. Ashworth et al.

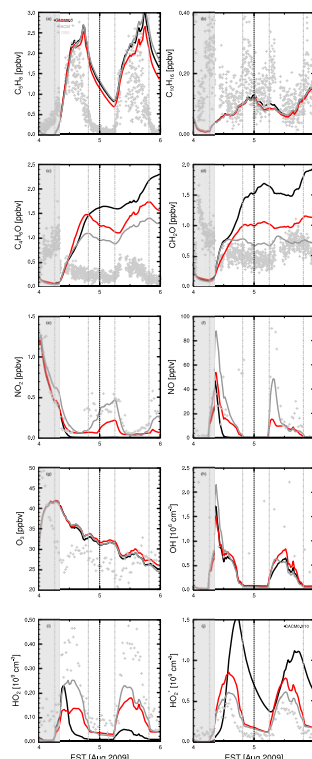


Figure 4. Concentrations of **(a)** isoprene, **(b)** summed monoterpenes, **(c)** MVK-MCR, **(d)** formaldehyde, **(e)** NO_2 , **(f)** NO , **(g)** ozone, **(h)** OH , **(i)** HO_2 , and **(j)** HO_2^* for 04–05 August 2009 at the top of the flux tower (corresponding to 36.94 m for model output data and 34 m for measurements). Model data from CACM are shown in red; measurement data by crosses. Data for CACM0.0 (black) and RACM (grey) are shown for comparison.

Title Page

Abstract

Introduction

Conclusions

References

Tables

Figures



Back

Close

Full Screen / Esc

Printer-friendly Version

Interactive Discussion



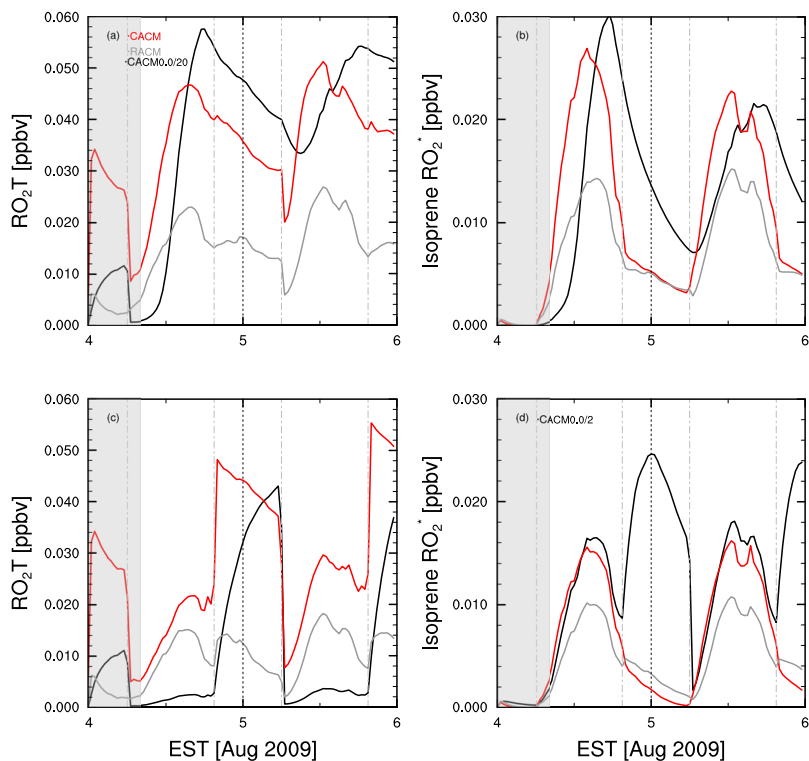


Figure 5. Concentrations of peroxy radicals at the top of the canopy (19.47 m for model output data, 20.4 m for observations for low- NO_x conditions (top) and high- NO_x conditions (bottom). The left panels show the total peroxy radical (RO_2T) and the right panels peroxy radicals formed from the reactions of isoprene + OH. The data shown are output from the simulation using the optimised CACM chemistry scheme (red) in addition to the original CACM scheme (black) and RACM scheme (grey). Note that the concentrations in the CACM base simulations are scaled by a factor of 20 in (a–c) and by 2 in (d).

FORest canopy atmosphere transfer (FORcAsT) 1.0

K. Ashworth et al.

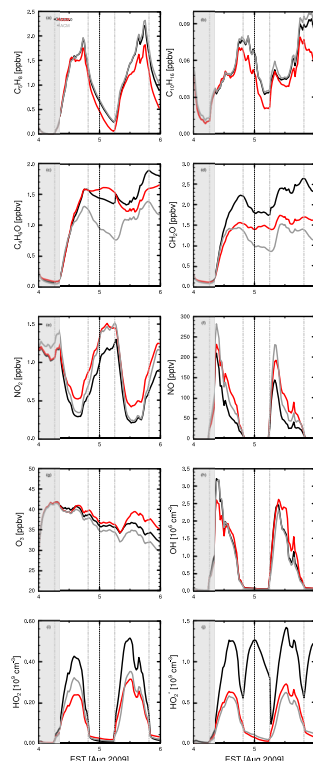


Figure 6. Concentrations of **(a)** isoprene, **(b)** summed monoterpenes, **(c)** MVK-MCR, **(d)** formaldehyde, **(e)** NO_2 , **(f)** NO , **(g)** ozone, **(h)** OH , **(i)** HO_2 , and **(j)** HO_2^* for 04–05 August 2009 at the top of the flux tower (corresponding to 36.94 m for model output data and 34 m for measurements). Data from CACM are shown in red, RACM grey, and CACM0.0 black.

Title Page

Abstract

Introduction

Conclusions

References

Tables

Figures



Back

Close

Full Screen / Esc

Printer-friendly Version

Interactive Discussion



FORest canopy
atmosphere transfer
(FORCAst) 1.0

K. Ashworth et al.

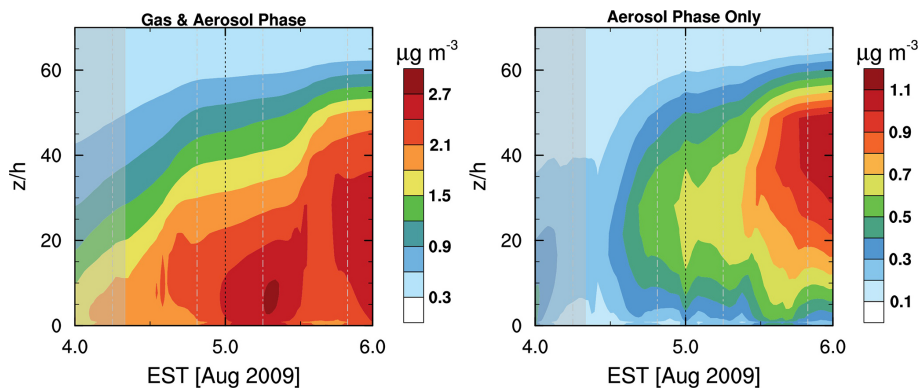


Figure 7. Modeled total condensable (left) and aerosol-phase (right) concentrations.

[Title Page](#)[Abstract](#)[Introduction](#)[Conclusions](#)[References](#)[Tables](#)[Figures](#)[Back](#)[Close](#)[Full Screen / Esc](#)[Printer-friendly Version](#)[Interactive Discussion](#)

FORest canopy
atmosphere transfer
(FORCAsT) 1.0

K. Ashworth et al.

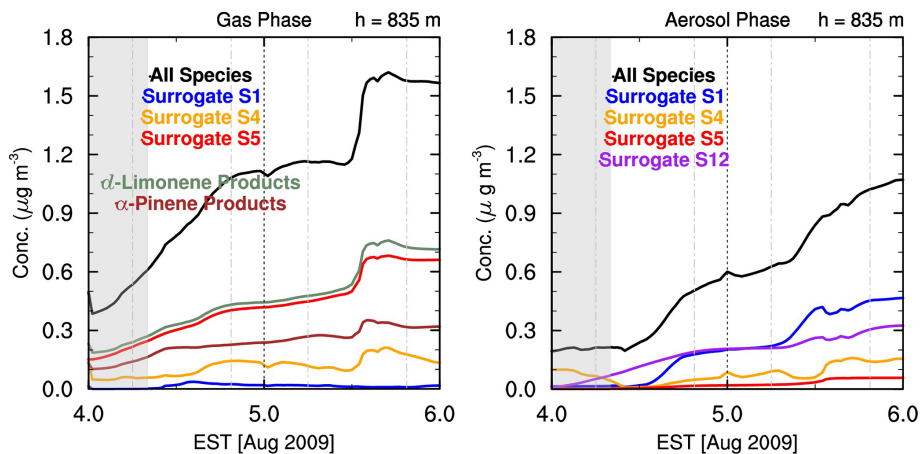


Figure 8. Modeled concentrations at 835 m in the gas (left) and aerosol (aerosol) phases.

[Title Page](#)[Abstract](#)[Introduction](#)[Conclusions](#)[References](#)[Tables](#)[Figures](#)[Back](#)[Close](#)[Full Screen / Esc](#)[Printer-friendly Version](#)[Interactive Discussion](#)